

The exon junction complex undergoes a compositional switch that alters mRNP structure and nonsense-mediated mRNA decay activity

Justin W. Mabin^{1,5,6}, Lauren A. Woodward^{1,5,6}, Robert Patton^{3,5,6}, Zhongxia Yi^{1,5}, Mengxuan Jia², Vicki Wysocki^{2,5}, Ralf Bundschuh^{3,4,5}, Guramrit Singh^{1,5,7*}

¹Department of Molecular Genetics, The Ohio State University, Columbus, OH 43210

²Department of Chemistry and Biochemistry, The Ohio State University, Columbus, OH 43210

³Department of Physics, The Ohio State University, Columbus, OH 43210

⁴Division of Hematology, Department of Internal Medicine, The Ohio State University, Columbus, OH 43210

⁵Center for RNA Biology, The Ohio State University, Columbus, OH 43210

⁶These authors equally contributed to this work

⁷Lead contact

*Correspondence: Guramrit Singh (singh.734@osu.edu)

SUMMARY

The exon junction complex (EJC) deposited upstream of mRNA exon junctions shapes structure, composition and fate of spliced mRNA ribonucleoprotein particles (mRNPs). To achieve this, the EJC core nucleates assembly of a dynamic shell of peripheral proteins that function in diverse post-transcriptional processes. To illuminate consequences of EJC composition change, we purified EJCs from human cells via peripheral proteins RNPS1 and CASC3. We show that EJC originates as an SR-rich mega-dalton sized RNP that contains RNPS1 but lacks CASC3. After mRNP export to the cytoplasm and before translation, the EJC undergoes a remarkable compositional and structural remodeling into an SR-devoid monomeric complex that contains CASC3. Surprisingly, RNPS1 is important for nonsense-mediated mRNA decay (NMD) in general whereas CASC3 is needed for NMD of only select mRNAs. The promotion of switch to CASC3-EJC slows down NMD. Overall, the EJC compositional switch dramatically alters mRNP structure and specifies two distinct phases of EJC-dependent NMD.

KEYWORDS

Ribonucleoproteins, exon junction complex, splicing, spliceosome, translation, ribosome, nonsense-mediated mRNA decay

INTRODUCTION

From the time of their birth during transcription until their eventual demise following translation, messenger RNAs (mRNA) exist decorated with proteins as mRNA-protein particles, or mRNPs (Gehring et al., 2017; Singh et al., 2015). The vast protein complement of mRNPs has been recently illuminated (Baltz et al., 2012; Castello et al., 2012; Hentze et al., 2018), and is believed to change as mRNPs progress through various life stages. However, the understanding of mechanisms and consequences of mRNP composition change remains confined to only a handful of its components. For example, mRNA export adapters are removed upon mRNP export to provide directionality to mRNP metabolic pathways, and the nuclear cap and poly(A)-tail binding proteins are exchanged for their cytoplasmic counterparts after mRNP export to promote translation (Singh et al., 2015, and references therein). When, where and how the multitude of mRNP components change during its lifetime, and how such changes impact mRNP function remain largely unknown.

A key component of all spliced mRNPs is the exon junction complex (EJC), which assembles during pre-mRNA splicing 24 nucleotides (nt) upstream of exon-exon junctions (Boehm and Gehring, 2016; Le Hir et al., 2016; Woodward et al., 2017). Once deposited, the EJC enhances gene expression at several post-transcriptional steps including pre-mRNA splicing, mRNA export, mRNA transport and localization, and translation. If an EJC remains bound to an mRNA downstream of a ribosome terminating translation, it stimulates rapid degradation of the mRNA via nonsense-mediated mRNA decay (NMD). The stable EJC core forms when RNA bound EIF4A3 is locked in place by RBM8A (also known as Y14) and MAGOH. It has been proposed that this trimeric complex is joined by a fourth protein CASC3 (also known as MLN51 or Barenstz) to form a stable tetrameric core (Boehm and Gehring, 2016; Hauer et al., 2016; Le Hir et al., 2016; Tange et al., 2005). However, more recent evidence suggests that CASC3 may not be present in all EJCs and may not be necessary for all EJC functions (Mao et al., 2017; Singh et al., 2012). Nonetheless, the stable EJC core is bound by a dynamic shell of peripheral EJC proteins such as pre-mRNA splicing factors (e.g. SRm160, RNPS1), mRNA export proteins (e.g. the TREX complex), translation factors (e.g. SKAR) and NMD factors (e.g. UPF3B) (Boehm and Gehring, 2016; Le Hir

et al., 2016; Woodward et al., 2017). Some peripheral EJC proteins share similar functions and yet may act on different mRNAs; e.g. RNPS1 and CASC3 can both enhance NMD but may have distinct mRNA targets (Gehring et al., 2005). Thus, the peripheral EJC shell may vary between mRNPs leading to compositionally distinct mRNPs, an idea that has largely remained untested.

We previously showed that within spliced mRNPs EJCs interact with one another as well as with several SR and SR-like proteins to assemble into mega-dalton sized RNPs (Singh et al., 2012). These stable mega RNPs ensheath RNA well beyond the canonical EJC deposition site leading to RNA footprints ranging from 150-200 nt in length, suggesting that the RNA polymer within these complexes is packaged resulting in overall compact mRNP structure. Such a compact structure may facilitate mRNP navigation of the intranuclear environment, export through the nuclear pore and transport within the cytoplasm to arrive at its site of translation. Eventually, the mRNA within mRNPs must be unpacked to allow access to the translation machinery. How long do mRNPs exist in their compact states, and when, where and how are they unfurled remains yet to be understood.

Our previous observation that in human embryonic kidney (HEK293) cells CASC3 and many peripheral EJC factors are substoichiometric to the EJC core (Singh et al., 2012) spurred us to investigate variability in EJC composition. Here we use EJC purification via substoichiometric factors to reveal that EJCs first assemble into SR-rich mega-dalton sized RNPs, and then undergo a compositional switch into SR-devoid monomeric CASC3-containing EJC. The translationally repressed mRNPs, particularly those encoding ribosomal proteins, accumulate with the CASC3-bound form of the EJC. Although both the EJC forms remain active in NMD, RNPS1, a component of the SR-rich EJCs, is crucial for all tested NMD events whereas CASC3, a constituent of SR-devoid EJC, is dispensable for NMD of many transcripts. Our findings reveal a new step in the mRNP life cycle wherein EJCs, and by extension mRNPs, undergo a remarkable compositional switch that alters the mRNP structure and specifies two distinct phases of EJC dependent NMD.

RESULTS

RNPS1 and CASC3 associate with the EJC core in a mutually exclusive manner

We reasoned that substoichiometric EJC proteins may not interact with all EJC cores, and therefore, some of them may not interact with each other leading to variable EJC composition. To test such a prediction, we carried out immunoprecipitations (IP) of either endogenous core factor EIF4A3 or the substoichiometric EJC proteins RNPS1 and CASC3 from RNase A-treated HEK293 total cell extracts. As expected, EIF4A3 IP enriches EJC core as well as all peripheral proteins tested (Figure 1A, lane 3). In contrast, the IPs of substoichiometric factors enriched only distinct sets of proteins. CASC3 immunopurified the EJC core proteins (EIF4A3, RBM8A and MAGOH) but not the peripheral proteins ACIN1 and SAP18 (Figure 1A, lane 4; RNPS1 could not be blotted for as it co-migrates with IgG heavy chain). Conversely, following RNPS1 IP, the EJC core proteins as well as its known binding partner SAP18 (Murachelli et al., 2012; Tange et al., 2005) were enriched but CASC3 was undetected in these IPs. We saw an identical lack of co-IP between RNPS1 and CASC3 from cells that were crosslinked with formaldehyde prior to lysis (data not shown; also see below), suggesting that the lack of interaction between these substoichiometric factors does not result from their dissociation following cell lysis. We also carried out similar IPs from RNase-treated total extracts from mouse brain cortical slices, mouse embryonal carcinoma (P19) cells, and HeLa cells. Again, both RNPS1 and CASC3 efficiently co-IPed with EIF4A3 from these lysates but no co-IP was detected between RNPS1 and CASC3 (compare lanes 4 and 5 with lane 3 in Figures 1B, S1A and S1B). Therefore, we conclude that in mammalian cells RNPS1 and CASC3 exist in complex with the EJC core in a mutually exclusive manner, and term these compositionally distinct EJCs as alternate EJCs.

Proteomic Analysis of Alternate EJCs

To gain insights into alternate compositions of the EJC, we further characterized RNPS1 and CASC3-containing complexes using a bottom-up proteomics approach. We generated HEK293 cell lines stably expressing FLAG-tagged RNPS1 and CASC3 from a tetracycline inducible promoter where the proteins are induced at near endogenous levels (Figure S1C). FLAG IPs from RNase-treated total extracts of FLAG-RNPS1 and

FLAG-CASC3 expressing cells confirmed that the tagged proteins also exist in mutually exclusive EJCs (Figure S1D). Importantly, proteomic analysis of FLAG-affinity purified alternate EJCs show almost complete lack of spectra corresponding to RNPS1 and CASC3 in the immunoprecipitates of the other alternate EJC factor (Figures 1C and S1E). In comparison, a FLAG-MAGOH IP enriches both CASC3 and RNPS1 as expected (Figures 1C, S1D and S1E).

We next compared the full complement of proteins associated with FLAG-RNPS1, FLAG-CASC3 and FLAG-MAGOH focusing on proteins >2-fold enriched in any one of the three EJC IPs as compared to the FLAG-only negative control (Table S1; see Experimental Procedures). Of the 59 proteins enriched in the two FLAG-RNPS1 biological replicates (Figure S2A), 38 are common with the 45 proteins identified in the two FLAG-MAGOH replicates (Figures S2A and S2B). Such a high degree of overlap suggests that RNPS1 containing complexes are compositionally similar to those purified via the EJC core. In comparison, among the two FLAG-CASC3 replicates the only common proteins are EIF4A3 and MAGOH (Figure S2A), which are also shared with FLAG-MAGOH (Figure S2C). Known EJC interactors such as UPF3B and PYM1 are identified in only one of the two FLAG-CASC3 replicates indicating less stable CASC3 association with these EJC factors.

A direct comparison of FLAG-RNPS1 and FLAG-CASC3 proteomes highlights their stark differences beyond the common EJC core (Figures 2A and 2B). Several SR and SR-like proteins are enriched in the RNPS1 and MAGOH proteomes but are completely absent from the CASC3 samples. Among the SR protein family, SRSF1, 6, 7 and 10 are reproducibly enriched in all RNPS1 and MAGOH samples, while all other canonical SR proteins, with the exception of non-shuttling SRSF2, are detected in at least one of the two replicates (Figure 2A, 2B, 2C and Table S1). Several SR-like proteins such as ACIN1, PNN, SRRM1 and SRRM2 are also highly enriched in MAGOH and RNPS1 IPs but are absent in CASC3 IPs (Figure 2 and Table S1). A weak but erratic signal for SRSF1 and SAP18 is seen in FLAG-CASC3 IPs (e.g. spectra for two SRSF1-derived peptides are observed in one of the FLAG-CASC3 samples; Figure 2B). However, their enrichment in CASC3-EJC is much weaker as compared to MAGOH or

RNPS1 samples. Overall, these findings suggest an extensive interaction network between SR and SR-like proteins and the RNPS1-EJC but not the CASC3-EJC.

The proteomes of the three EJC factors can be readily classified based on protein functions in RNA biogenesis, their assembly/function within RNPs, or their protein sequence composition (Figure 2B). Many RNA biogenesis factors are specifically associated with RNPS1 (and MAGOH) but not with CASC3. These include transcription machinery components (e.g. RPB1, RPB2), transcriptional regulators (e.g. CD11A, CDK12) as well as RNA processing factors (e.g. NCBP1, FIP1). Consistent with EJC core assembly during pre-mRNA splicing, MAGOH and RNPS1 interactors also include U2, U4 and U6 snRNP components and nineteen complex subunits. None of the splicing components are seen to interact with CASC3. Considering that SR proteins also assemble onto nascent RNAs co-incident with transcription and splicing (Zhong et al., 2009), the EJC-RNPS1-SR interaction network likely originates during co-transcriptional mRNP biogenesis. In contrast, CASC3 most likely engages with the EJC only post-splicing, as previously suggested (Gehring et al., 2009a).

Alternate EJCs differ in their higher order structure

The enrichment of SR and SR-like proteins exclusively with RNPS1 suggested that RNPS1 EJCs are likely to resemble the previously described higher order EJCs (Singh et al., 2012). Indeed, glycerol gradient fractionation of RNase-treated complexes immunopurified via FLAG-RNPS1 shows that, like EJCs purified via FLAG-MAGOH, FLAG-RNPS1 EJCs contain both lower and higher molecular weight complexes (Figure 2D). On the other hand CASC3 is mainly detected in lower molecular weight complexes purified via FLAG-MAGOH (Figure 2D, compare CASC3 signal in fractions 2-10 and 22-24). Furthermore, complexes purified via FLAG-CASC3 are exclusively comprised of lower molecular weight complexes, likely to be EJC monomers (Figure 2D). These findings are consistent with the proteomic results and suggest that compositional distinctions between the two alternate EJCs give rise to two structurally distinct complexes.

RNPS1 and CASC3 bind RNA via the EJC core with key distinctions

We next identified the RNA binding sites for the two alternate EJC factors using RNA:protein immunoprecipitation in tandem (RIPiT) combined with high-throughput sequencing, or RIPiT-Seq (Singh et al., 2012, 2014). RIPiT-Seq entails tandem purification of two subunits of an RNP, and is well-suited to study EJC composition via sequential IP of its constant (e.g. EIF4A3, MAGOH) and variable (e.g. RNPS1, CASC3) components (Figure 3A). We carried out RIPiTs from HEK293 cells by either pulling first on FLAG-tagged alternate EJC factor followed by IP of an endogenous core factor, or vice versa. As a control, we also performed FLAG-MAGOH:EIF4A3 RIPiT-Seq. All *in vivo* EJC binding studies thus far have employed a short incubation with translation elongation inhibitor cycloheximide prior to cell lysis to limit EJC disassembly by translating ribosomes (Hauer et al., 2016; Saulière et al., 2012; Singh et al., 2012). However, to capture unperturbed, steady-state populations of RNPS1 and CASC3 bound EJCs (as in Figures 1 and 2), we performed RIPiT-Seq without translation inhibition.

As expected, RIPiTs for each of the two alternate EJCs specifically purified the targeted complex along with the EJC core factors and yielded abundant RNA footprints (Figure S3A). Strand-specific RIPiT-Seq libraries from ~35-60 nucleotide footprints yielded ~5.7 to 47 million reads, of which >80% mapped uniquely to the human genome (hg38; Table S2). Genic read counts are highly correlated between RIPiTs where the order of IP of EJC core and alternate factors was reversed (Figures S3B and S3C). We found that RNPS1-EJC core interaction is susceptible to NaCl concentrations greater than 250 mM whereas CASC3-EJC core interaction persists up to 600 mM NaCl (data not shown). Therefore, to preserve labile interactions we performed alternate EJC RIPiTs from cells cross-linked with formaldehyde before cell lysis (Figure S3D). We observed a strong correlation for genic read counts between crosslinked and uncrosslinked samples (Figures S3E and S3F). The analysis presented below is from two well-correlated biological replicates of formaldehyde crosslinked RIPiT-Seq datasets of RNPS1- and CASC3-EJC (Figures S3G and S3H).

Consistent with EJC deposition on spliced RNAs, alternate EJC footprints are enriched in exonic sequences from multi-exon genes (Figure S3I). Along individual

exons, footprints of both alternate EJCs mainly occur close to exon 3' ends (Figure 3B). Indeed, a meta-exon analysis shows that the alternate EJC factors bind mainly to the canonical EJC binding site 24 nt upstream of exon junctions (Figure 3C) (Hauer et al., 2016; Saulière et al., 2012; Singh et al., 2012). Notably, the alternate EJC footprint enrichment at the canonical EJC site is irrespective of whether the alternate EJC factors are IPed first or second during the RIPiT procedure (Figure S3J). Thus, both RNPS1 and CASC3 mainly bind to RNA via EJCs at the canonical site. The location of the 5'- and 3'-ends of the alternate EJC footprint reads shows that both alternate EJCs have a similar footprint on RNA as each blocks positions -26 to -19 nt from RNase I cleavage (Figure 3D). Our findings are consistent with previous work that showed that CASC3 mainly binds to the canonical EJC site (Hauer et al., 2016). However, in contrast to this study, RNPS1 binding to canonical EJC sites is readily apparent (Figures 3B, 3C and 3D), which could reflect differences in the UV-crosslinking dependent CLIP-Seq approach used by Hauer *et al.* and the photo-crosslinking independent RIPiT-Seq. Altogether, our results suggest that both RNPS1 and CASC3 exist in complex with EJC at its canonical site.

While read densities for both alternate EJC factors are highest at the canonical EJC site, 47-62% of reads map outside of the canonical EJC site similar to previous estimates (Saulière et al., 2012; Singh et al., 2012). Non-canonical footprints are somewhat more prevalent in RNPS1-EJC as compared to CASC3-EJC (Figure S3K). As RNPS1-EJC is intimately associated with SR and SR-like proteins (Figure 2A and B), a k-mer enrichment analysis revealed a modest but significant enrichment of GA-rich 6-mers in RNPS1 over CASC3 footprints (Figures 3E). Such purine-rich sequences occur in binding sites of several SR proteins (SRSF1, SRSF4, Tra2a and b) (Änkö et al., 2012; Pandit et al., 2013; Tacke et al., 1998). There is also a small but significant enrichment of sequence motifs recognized by SRSF1 and SRSF9 in RNPS1 footprints as compared to CASC3 footprints or RNA-Seq reads (Figures 3F, 3G, S3L and S3M). We conclude that within spliced RNPs, RNPS1-containing EJC is engaged with SR and SR-like proteins, and other RNA binding proteins, which leads to co-enrichment of RNA binding sites of these proteins during RIPiT via RNPS1. Intriguingly, CG-rich 3-mers are the highest enriched k-mers in footprints of both alternate EJCs as compared to RNA-

Seq (data not shown). The CG-rich 6-mers are also somewhat more enriched in RNPS1-EJC (Figure 3E). A CG-rich sequence was reported as an *in vitro* RBM8A binding motif indicating a yet to be determined relationship between the EJC core and CG-rich sequences (Ray et al., 2013).

RNPS1 and CASC3 RNA occupancy changes with mRNP subcellular location

Surprisingly, despite the mutually exclusive association of RNPS1 and CASC3 with the EJC core (Figures 1 and 2), the two proteins are often detected on the same sites on RNA leading to their similar apparent occupancy on individual exons as well as entire transcripts (Figures 3B, S4A and S4B). These results suggest that the two alternate EJC factors bind to two distinct pools of the same RNAs. To further reveal RNA binding patterns of the alternate EJC factors, we first identified exons differentially enriched in one or the other factor. Remarkably, if two or more exons of the same gene are differentially enriched in RNPS1 or CASC3 footprints, these exons are almost always enriched in the same alternate EJC factor (Figure 4A, $p < 0.00001$). This extremely tight linkage between EJC compositions of different exons of the same gene suggests that RNPS1 and CASC3 binding to EJC is determined at the level of the entire transcript and not of the individual exon. At any given time a transcript with multiple EJCs is likely to be homogeneously associated with either one or the other alternate factor. In support of this scenario, very weak RNA-dependent interaction is detected between the two alternate EJC factors (Figure S4C).

At steady state, RNPS1 is mainly localized to the nucleus whereas CASC3 is predominantly cytoplasmic although both proteins shuttle between the two compartments (Daguenet et al., 2012; Degot et al., 2002; Lykke-Andersen et al., 2001). We reasoned that different concentration of alternate EJC factors in the two subcellular compartments may mirror their EJC association and RNA occupancy. To test this possibility, we identified subsets of transcripts that are preferentially enriched in RNPS1-EJC (242 transcripts) or CASC3-EJC (625 transcripts; Figure 4B), and compared their nuclear:cytoplasmic ratios based on estimates of subcellular RNA distribution in HEK293 cells (Neve et al., 2016). Indeed, the transcripts enriched in CASC3-EJC strongly localize to the cytoplasm (median % localized in cytoplasm = 76), whereas

those preferentially bound to RNPS1 show more even distribution with a slight bias for nuclear localization (median % localized in cytoplasm = 48; Figures 4C and S4D). Thus, subcellular localization of spliced RNAs and EJC factors are important determinants of EJC composition.

We surmised that kinetics of mRNA maturation and in turn nuclear export will directly impact EJC composition. To test this idea, we compared alternate EJC occupancy of a group of genes whose nuclear poly(A)-tailed transcripts contain introns that undergo splicing much more slowly as compared to other introns in the same transcript (Boutz et al., 2015). Transcripts containing these detained introns (DI) are restricted to the nucleus in a mostly pre-processed state until DIs are spliced, and are therefore expected to have slower mRNA export rates. Of the genes that Boutz *et al.* found to contain DI in four human cell lines, 542 also contained DIs in HEK293 cells whereas a set of 389 transcripts do not contain DI in any human cell lines including HEK293 cells (data not shown). We find that DI-containing transcripts are significantly more enriched in RNPS1-EJC ($p=8.3 \times 10^{-13}$, Figures 4D and 4E) while DI lacking transcripts show an enrichment in CASC3-EJC ($p=1.8 \times 10^{-7}$). These results support our conclusion that EJC (and mRNP) compositional switch mainly occurs as they mature and enter the cytoplasm, and that the rate of mRNA progression to the cytoplasm alters the switch.

Despite a strong CASC3 enrichment on cytoplasmic RNAs, a quarter of all preferentially CASC3-bound RNAs are more nuclear (Figure 4C). Consistent with CASC3 shuttling into the nucleus (Daguenet et al., 2012; Degot et al., 2002), its footprints are abundantly detected on *XIST* RNA and several other spliced non-coding RNAs restricted or enriched in the nucleus (Figures 4F and S4D). Further, in HEK293 nuclear as well as cytoplasmic extracts both CASC3 and RNPS1 are found to assemble into EJCs (Figures S4E and S4F). These data suggest that while the bulk of RNPs may undergo the switch in EJC composition in the cytoplasm, some RNPs can undergo this change in the nucleus itself, possibly as a function of RNP half-life or due to a more active nuclear role of CASC3 in RNP biogenesis and function.

Translation and mRNA decay kinetics impacts alternate EJC bound mRNA pools

As EJCs are disassembled during translation (Dostie and Dreyfuss, 2002; Gehring et al., 2009b), abundant RNPS1 and CASC3 footprints at EJC deposition sites suggest that the bulk of mRNPs undergo the compositional switch before translation. To test how translation impacts occupancy of both alternate EJCs, and if their occupancy is influenced by rate at which mRNAs enter translation pool, we obtained RNPS1- and CASC3-EJC footprints from cells treated with cycloheximide (CHX), and compared them to alternate EJC footprints from untreated cells. When mRNAs bound to each alternate EJC are compared across the two conditions, CASC3 RNA occupancy shows a dramatic change (Figure 5A). In contrast, while changes in RNPS1-bound RNAs across two conditions shows the same trend as CASC3 ($R^2=0.27$, Figure 5A), the change is much less dramatic with RNPS1 occupancy changing significantly only on a handful of transcripts. These observations further support our conclusion that the RNPS1-bound form of the EJC precedes the CASC3-bound form. They also indicate that translation inhibition does not interfere with the compositional switch from RNPS1 to CASC3 but leads to accumulation of CASC3-bound mRNPs.

It is expected that poorly translated or translationally repressed mRNAs will be enriched in CASC3-EJC under normal conditions, and more efficiently translated mRNAs will be differentially enriched upon translation inhibition. To test this hypothesis, we obtained mRNA translation efficiency (TE) estimates based on ribosome footprint counts for each transcript normalized to its abundance from a human colorectal cancer cell line (Kiss et al., 2017). A comparison of the CASC3-EJC enriched transcripts from the two conditions however showed only a minor difference in their median TE (Figure S5A). A search for functionally related genes in the two sets revealed that each contains diverse groups (Figure 5B). Among the transcripts differentially bound to CASC3-EJC under normal conditions, the largest and most significantly enriched group encodes signal-peptide bearing secretory/membrane bound proteins (Figure 5B), which has a significantly higher TE as compared to all transcripts (Figure S5B). We reason that despite the higher TE of the “secretome” (all secreted/membrane proteins as classified in (Jan et al., 2014)), transcripts with signal peptide may be enriched in CASC3-EJC because binding of the hydrophobic signal peptide to the signal recognition particle halts

translation, which resumes only when the ribosome engages with the endoplasmic reticulum (ER) (Walter and Blobel, 1981). Presumably, the time before translation resumption on the ER allows capture of mRNPs where EJC composition has switched but the complex has not yet been disassembled by translation. When we excluded the secretome and considered only those transcripts that are translated in the cytosol (as defined in (Chen et al., 2011)), a comparison of TE of CASC3-EJC enriched transcripts under translation conducive and inhibitory conditions confirmed our initial hypothesis. As seen in Figure 5C, transcripts bound to CASC3-EJC in the absence of CHX have significantly lower median TE (-2.56) as compared to median TE of transcripts bound to CASC3-EJC in the presence of CHX (-2.08, $p=2.7 \times 10^{-4}$).

Another functional group enriched in CASC3-EJC under normal conditions comprises the ribosomal protein (RP)-coding mRNAs (Figure 5B). Strikingly, transcripts encoding ~50% of all cytosolic ribosomal subunit proteins as well as 13 mitochondrial ribosome subunits are among this set (Figure 5A). Although RP mRNAs are among the most highly translated in the cell, a sizeable fraction of RP mRNAs are known to exist in a dormant untranslated state that can enter the translation pool upon demand (Geyer et al., 1982; Meyuhas and Kahan, 2015; Patursky-Polischuk et al., 2009). Consistently, RP mRNAs have significantly low TE in human and mouse cells (Figures S5B and S5C). Furthermore, when transcripts differentially bound to RNPS1- versus CASC3-EJC are directly compared in normally translating cells, RP mRNAs are specifically enriched among CASC3-EJC bound transcripts (Figure 5D). Therefore, RP mRNPs, and perhaps other translationally repressed mRNPs, that linger in the untranslated state in the cytoplasm switch to and persist in the CASC3-bound form of the EJC. Such a possibility is further supported by significantly lower TE of CASC3-EJC enriched RNAs as compared to RNPS1-EJC bound transcripts under normal conditions (Figure 5E). Further, when mRNPs are forced to persist in an untranslated state upon CHX treatment, cytosol translated mRNAs show increased CASC3 occupancy whereas their RNPS1 occupancy is not affected (Figure S5D).

As previously reported (Hauer et al., 2016), RP mRNAs are depleted of CASC3-EJC upon translation inhibition (Figures 5A and 5D). Upon cycloheximide treatment, CASC3 occupancy is significantly reduced at canonical EJC sites of RP mRNAs as

compared to non-RP mRNAs, which show an increase in CASC3 occupancy (Figure 5F, $p=2.5 \times 10^{-43}$). In comparison, RNPS1 occupancy on all transcripts modestly increases upon translation inhibition (Figure 5F, $p=0.059$). A paradoxical possibility is that the untranslated reserves of RP mRNAs may undergo translation when the cellular pool of free ribosomes is dramatically reduced upon CHX-mediated arrest of translating ribosomes on mRNAs. Intriguingly, a recent study in fission yeast found a similar contradictory increase in ribosome footprint densities on RP mRNAs upon cycloheximide treatment (Duncan and Mata, 2017).

The alternate EJC occupancy landscape is also impacted by mRNA decay kinetics. CASC3-EJC enriched RNAs have longer half-lives as compared to RNPS1-EJC enriched transcripts under both translation conducive (median $t_{1/2}=4.6$ hr vs. 5.9 hr, $p=3.1 \times 10^{-3}$) and inhibitory conditions (median $t_{1/2}=3.4$ hr vs. 4.8 hr, $p=5.3 \times 10^{-5}$, Figure 5G). Notably, RNAs enriched in both alternate EJCs upon CHX treatment have lower half-lives as compared to the corresponding cohorts enriched from normal conditions. Thus, EJC detection is enhanced on transcripts that are stabilized after CHX treatment. Such a conclusion is further supported by enrichment of functionally related groups of genes known to encode unstable transcripts (e.g. cell cycle, mRNA processing and DNA damage, (Schwanhäusser et al., 2011)) in CASC3-EJC upon translation inhibition (Figure 5B).

RNPS1 is required for efficient NMD of all transcripts whereas CASC3 is dispensable for many

Our data suggests that mRNPs arrive in the cytoplasm with RNPS1 and SR protein-containing EJCs, which are remodeled into CASC3-containing EJCs. We wanted to determine if alternate EJCs were equally important for NMD and/or if they have distinct targets as previously suggested (Gehring et al., 2005). In HEK293 cells with ~80% of RNPS1 mRNA and proteins depleted, a majority of endogenous NMD targets tested are significantly upregulated (Figures 6A and S6A). Surprisingly, however, in cells with ~85% of CASC3 depleted, NMD targets are largely unaffected; some others are only modestly upregulated, and only one out of thirteen is significantly upregulated. Notably, the RNAs that were upregulated upon CASC3 depletion are even more upregulated

upon RNPS1 depletion. Most tested RNAs are significantly upregulated upon depletion of EIF4A3 and the central NMD factor UPF1 (Figure 6A and data not shown). These data suggest that RNPS1 function is required for efficient NMD of most endogenous NMD substrates whereas CASC3 may be needed for NMD of only select RNAs.

It is possible that the residual amount of CASC3 after its siRNA mediated depletion is sufficient to support NMD. To test this further, we depleted endogenous EIF4A3 protein to ~50% of its normal levels and supplemented cells with either a WT EIF4A3 (WT) or an EIF4A3 mutant (YRAA: Y205A, R206A) with much reduced CASC3 binding (Figures 6B, S6B, S6C, S6D, (Andersen et al., 2006; Ballut et al., 2005; Bono et al., 2006). The EIF4A3 knockdown results in >2-fold upregulation of all NMD targets tested (Figure 6B). We find that complementation of EIF4A3 knockdown cells with exogenous FLAG-EIF4A3 or FLAG-EIF4A3 YRAA proteins leads to nearly identical effect on NMD restoration (Figure 6B). Based on the degree of rescue, the NMD targets tested can be divided into two groups. The first group (to the left of vertical red dotted line in Figure 6B) shows a strong rescue of NMD upon complementation with both the wild-type or the mutant EIF4A3 proteins. Therefore, this group of transcripts can undergo NMD largely independent of CASC3. In the second group (to the right of vertical red dotted line in Figure 6B), neither the wild-type nor the mutant proteins can rescue NMD defect caused by the depletion of endogenous EIF4A3 protein. We noted that, unlike the first group (with exception of C1orf37), the second group is somewhat more sensitive to depletion of CASC3 (Figure 6A). This subset of mRNAs may have a more complex dependence on EIF4A3 levels.

In contrast to most endogenous NMD substrates, we found that knockdown of both RNPS1 and CASC3 in HeLa cells leads to accumulation of a well-known β -globin mRNA with a premature stop codon at codon 39 (β 39, Figures 6C and S6E). Consistently, recent genome-wide screens have identified CASC3 as an effector of NMD of exogenous reporters (Alexandrov et al., 2017; Baird et al., 2018). Overall, our results show that, in human cells, several NMD targets can undergo CASC3 independent NMD whereas almost all tested transcripts depend on RNPS1 for their efficient NMD. On the other hand, exogenously (over) expressed NMD substrates may depend on both sequential EJC compositions for their efficient NMD.

Increased CASC3 levels slow down NMD

We next tested if overexpression of RNPS1 or CASC3 can tilt EJC composition toward one of the two alternate EJCs, and if such a change can impact NMD. CASC3 overexpression in HEK293 cells leads to several fold increase in CASC3 co-IP with EIF4A3 (Figures 7A, 7B) and RBM8A (Figures S7A and S7B), although no concomitant decrease is seen in RNPS1 co-precipitation with EJC core proteins. Consistent with this, manifold overexpression of RNPS1 did not cause any detectable change in levels of the two alternate factors in the EJC core IPs (Figures 7A, 7B and S7A and S7B). These results rule out a simple, direct competition between the two proteins for EJC core interaction. We next tested if increased CASC3 association with EJCs under elevated CASC3 levels affects NMD. Surprisingly, more than half of tested endogenous NMD targets are significantly upregulated upon CASC3 overexpression (Figure 7C). Similarly, the β 39 mRNA exogenously expressed in HeLa cells is also modestly stabilized upon CASC3 overexpression (Figure 7D and S7C). As previously reported (Viegas et al., 2007), RNPS1 overexpression further downregulates β 39 mRNA in HeLa cells (Figures S7C and S7D), indicating that NMD of this RNA occurs more efficiently when it is associated with early acting SR-rich EJC.

DISCUSSION

The EJC is a cornerstone of all spliced mRNPs, and interacts with upwards of 50 proteins to connect the bound RNA to a wide variety of post-transcriptional events. The EJC is thus widely presumed to be “dynamic”. By purifying EJC via key peripheral proteins, we demonstrate that a remarkable binary switch occurs in EJC’s complement of bound proteins. Such an EJC composition change has important implications for mRNP structure and function including mRNA regulation via NMD (Figure 7E).

EJC composition and mRNP structure

Our findings suggests that when EJCs first assemble during co-transcriptional splicing, the core complex consisting of EIF4A3, RBM8A and MAGOH engages with SR proteins and SR-like factors including RNPS1 (Figure 2). Within these complexes, RNPS1 is likely bound to both the EJC core as well as to the SR and SR-like proteins bound to their cognate binding sites on the RNA (Figure 3). This network of interactions bridges adjacent and distant stretches of mRNA, winding the mRNA up into a higher-order structure, which is characteristic of RNPs purified from human cells via the EJC core proteins or RNPS1 (Figure 2, (Singh et al., 2012)). Such higher-order mRNA packaging can create a compact RNP particle for its efficient intracellular transport. It is possible that assembly of these higher-order structures occur via multiple weak interactions among low complexity sequences (LCS) within EJC bound SR and SR-like proteins (Haynes and Iakoucheva, 2006; Kwon et al., 2014). It also remains to be tested if RNPS1, which possesses an SR-rich LCS, acts as a bridge between the EJC core and more distantly bound SR proteins. Our data also indicates that on a majority of mRNPs, these SR-rich and RNPS1-containing higher-order EJCs persist throughout their nuclear lifetime (Figure 4). When mRNPs arrive in the cytoplasm, the SR and SR-like proteins are evicted from all EJCs of an mRNP and the EJC is joined by CASC3 (Figure 4). It remains to be seen if CASC3 incorporation into an EJC causes its remodeling. Alternatively, active process(es) such as RNP modification via SR protein phosphorylation by cytoplasmic SR protein kinases (Zhou and Fu, 2013) or RNP remodeling by ATPases may precede CASC3 binding to EJC (Lee and Lykke-Andersen, 2013). What is clear is that CASC3-bound EJCs lose their higher order

structure and exist as monomeric complexes at the sites where EJC cores were co-transcriptionally deposited. Thus, the switch in EJC composition from RNPS1 and SR-rich complexes to CASC3-bound complexes leads to a striking alteration in higher-order EJC, and possibly, mRNP structure (Figure 7E). The CASC3 bound form of the EJC following compositional switch is the main target of translation dependent disassembly although RNPS1-EJC may undergo some translation-dependent disassembly (Figure 5).

CASC3-EJC and pre-translation mRNPs

Our findings support the emerging view that CASC3 is not an obligate component of all EJC cores. A population of assembled EJCs, especially those early in their lifetime, completely lack CASC3 (Figures 1 and 2). Such a view of partial CASC3 dispensability for EJC structure and function is in agreement with findings from *Drosophila* where the assembled trimeric EJC core as well as RNPS1 and its partner ACIN1 are required for splicing of long or sub-optimal introns whereas CASC3 is not (Hayashi et al., 2014; Malone et al., 2014; Roignant and Treisman, 2010). A recent report that lack of CASC3 during mouse embryonic brain development results in phenotypes distinct from those caused by similar mutations of the other three core proteins also supports non-overlapping functions of CASC3 and the other core factors (Mao et al., 2017). We note that in the recently reported human spliceosome C* structure, CASC3 is bound to the trimeric core (Zhang et al., 2017). As the spliceosomes described in these structural studies were assembled *in vitro* in nuclear extracts, it is possible that CASC3 present in extracts can enter pre-assembled spliceosomes and interact with EJC. Consistently, in the human spliceosome C* structure one of the two CASC3 binding surfaces on EIF4A3 is exposed and available for CASC3 interaction. Still, a possibility remains that, at least on some RNAs or exon junctions, CASC3 assembly may occur soon after splicing within peripsekles as previously suggested (Daguenet et al., 2012).

CASC3 is a more prominent component of cytoplasmic EJCs within mRNPs that have not yet been translated or are undergoing their first round of translation (Figure 5). Previously described functions of CASC3 within translationally repressed neuronal transport granules (Macchi et al., 2003) and posterior-pole localized *oskar* mRNPs in

Drosophila oocytes (van Eeden et al., 2001) further support CASC3 being a component of cytoplasmic pre-translation mRNPs. It remains to be tested if, like its active role in *oskar* mRNA localization and translation repression (van Eeden et al., 2001), CASC3 also plays a direct role in translational quiescence of RP mRNAs and/or their mobilization to rapidly meet increased demand for translation apparatus (Geyer et al., 1982; Patursky-Polischuk et al., 2009). Nonetheless, our results emphasize the idea of post-transcriptional regulons wherein mRNPs encoding functionally related activities are under coordinated translational control. Capture of such regulons via CASC3-EJC highlights a potential utility of EJC as a molecular marker to identify coordinately translated regulons, perhaps as a complementary approach to the recently described translation-dependent protein knock-off to monitor first round of translation of single mRNPs (Halstead et al., 2015).

EJC composition and NMD

Based on the binary EJC composition switch, EJC-dependent steps in the NMD pathway can be divided into at least two phases wherein the two alternate factors perform distinct functions. The susceptibility of all tested NMD targets to RNPS1 levels suggests that this protein, and perhaps other components of SR-rich EJCs, serve a critical function in an early phase in the pathway. Such a function could be to recruit and/or activate other EJC/UPF factors either in the nucleus or even during premature translation termination as part of the downstream EJC. Following the compositional switch, the EJC core maintains the ability to activate NMD as it can directly communicate with the NMD machinery via UPF3B (Buchwald et al., 2010; Chamieh et al., 2008). Still, following CASC3 incorporation into the EJC, its ability to stimulate NMD is likely reduced. Such a reduction may stem from the loss of RNPS1 or SR proteins, which are known to enhance NMD (Figure S7, (Aznarez et al., 2018; Sato et al., 2008; Viegas et al., 2007; Zhang and Krainer, 2004)). It is possible that CASC3 overexpression causes the compositional switch to occur at a faster rate or on a greater proportion of mRNAs, or both. Nevertheless, (over)expressed NMD reporters (e.g. β 39 mRNA) and some endogenous mRNAs depend on both early and late EJC compositions for their NMD. Notably, the β -globin NMD reporter was previously shown

to undergo biphasic decay with faster turnover around the nuclear periphery and slower decay in more distant cytoplasmic regions (Trcek et al., 2013). More recently, single-molecule imaging of reporter RNPs showed that a fraction of their population diffuses for several minutes and micrometers away from the nucleus before undergoing first round of translation (Halstead et al., 2015). It remains to be seen if mRNPs that are first translated in distant cytoplasmic locales, including those localized to specialized compartments such as neuronal dendrites and growth cones, may rely more on a CASC3-dependent slower phase of NMD. The EJC compositional switch may also underlie the distinct NMD branches identified earlier via tethering of RNPS1 and CASC3 to reporter mRNAs (Gehring et al., 2005). Consistent with these observations, we find that RNPS1 co-purifies more strongly with UPF2, while CASC3 appears to interact more with UPF3B (Figure 2 and data not shown). The nature of the relationship between EJC composition and UPF2 and UPF3B-independent NMD branches is an important avenue for the future work.

ACKNOWLEDGEMENTS

We would like to thank Pearly Yan and the OSU Comprehensive Cancer Center genomics core for high-throughput sequencing, Philip Sharp and Paul Boutz for detained-intron datasets, Daniel Schoenberg for H1299 cell line Ribo-Seq and RNA-Seq datasets for translation efficiency estimation, Jens Lykke-Andersen for plasmids and antibodies, Akila Mayeda for anti-RNPS1 antibody, Can Cenik for advice, and Anita Hopper for comments on the manuscript. This work was supported in part by an allocation from the Ohio Supercomputer Center. Funding for this work was provided by the Ohio State University and National Institutes of Health (R01-GM120209) to G.S.

AUTHOR CONTRIBUTIONS

Conceptualization, G.S. and R.B.; Investigation, J.W.M., L.A.W., R.P., Z.Y., M.J., and G.S.; Writing – Original Draft, G.S., J.W.M. and L.A.W.; Writing – Review & Editing, G.S., J.W.M., L.A.W., R.P., Z.Y., M.J., V.W. and R.B.; Funding Acquisition, G.S.; Resources, G.S., V.W. and R.B.; Supervision, G.S., V.W. and R.B.

DECLARATION OF INTERESTS

The authors declare no competing interests.

DATA AVAILABILITY

All high-throughput DNA sequencing data are being submitted to GEO and will be available upon publication under Bioproject PRJNA471492.

REFERENCES

- Alexandrov, A., Shu, M.-D., and Steitz, J.A. (2017). Fluorescence Amplification Method for Forward Genetic Discovery of Factors in Human mRNA Degradation. *Mol. Cell* **65**, 191–201.
- Andersen, C.B.F., Ballut, L., Johansen, J.S., Chamieh, H., Nielsen, K.H., Oliveira, C.L.P., Pedersen, J.S., Séraphin, B., Le Hir, H., and Andersen, G.R. (2006). Structure of the exon junction core complex with a trapped DEAD-box ATPase bound to RNA. *Science* **313**, 1968–1972.
- Änkö, M.-L., Müller-McNicoll, M., Brandl, H., Curk, T., Gorup, C., Henry, I., Ule, J., and Neugebauer, K.M. (2012). The RNA-binding landscapes of two SR proteins reveal unique functions and binding to diverse RNA classes. *Genome Biol.* **13**, R17.
- Aznarez, I., Nomakuchi, T.T., Tetenbaum-Novatt, J., Rahman, M.A., Fregoso, O., Rees, H., and Krainer, A.R. (2018). Mechanism of Nonsense-Mediated mRNA Decay Stimulation by Splicing Factor SRSF1. *Cell Rep.* **23**, 2186–2198.
- Baird, T.D., Cheng, K.C.-C., Chen, Y.-C., Buehler, E., Martin, S.E., Inglese, J., and Hogg, J.R. (2018). ICE1 promotes the link between splicing and nonsense-mediated mRNA decay. *Elife* **7**.
- Ballut, L., Marchadier, B., Baguet, A., Tomasetto, C., Séraphin, B., and Le Hir, H. (2005). The exon junction core complex is locked onto RNA by inhibition of eIF4AIII ATPase activity. *Nat. Struct. Mol. Biol.* **12**, 861–869.
- Baltz, A.G., Munschauer, M., Schwanhäusser, B., Vasile, A., Murakawa, Y., Schueler, M., Youngs, N., Penfold-Brown, D., Drew, K., Milek, M., et al. (2012). The mRNA-bound proteome and its global occupancy profile on protein-coding transcripts. *Mol. Cell* **46**, 674–690.
- Boehm, V., and Gehring, N.H. (2016). Exon Junction Complexes: Supervising the Gene Expression Assembly Line. *Trends Genet.* **32**, 724–735.
- Bono, F., Ebert, J., Lorentzen, E., and Conti, E. (2006). The crystal structure of the exon junction complex reveals how it maintains a stable grip on mRNA. *Cell* **126**, 713–725.
- Boutz, P.L., Bhutkar, A., and Sharp, P.A. (2015). Detained introns are a novel, widespread class of post-transcriptionally spliced introns. *Genes Dev.* **29**, 63–80.
- Buchwald, G., Ebert, J., Basquin, C., Sauliere, J., Jayachandran, U., Bono, F., Le Hir, H., and

Conti, E. (2010). Insights into the recruitment of the NMD machinery from the crystal structure of a core EJC-UPF3b complex. *Proc. Natl. Acad. Sci. U. S. A.* *107*, 10050–10055.

Castello, A., Fischer, B., Eichelbaum, K., Horos, R., Beckmann, B.M., Strein, C., Davey, N.E., Humphreys, D.T., Preiss, T., Steinmetz, L.M., et al. (2012). Insights into RNA biology from an atlas of mammalian mRNA-binding proteins. *Cell* *149*, 1393–1406.

Chamieh, H., Ballut, L., Bonneau, F., and Le Hir, H. (2008). NMD factors UPF2 and UPF3 bridge UPF1 to the exon junction complex and stimulate its RNA helicase activity. *Nat. Struct. Mol. Biol.* *15*, 85–93.

Chen, Q., Jagannathan, S., Reid, D.W., Zheng, T., and Nicchitta, C.V. (2011). Hierarchical regulation of mRNA partitioning between the cytoplasm and the endoplasmic reticulum of mammalian cells. *Mol. Biol. Cell* *22*, 2646–2658.

Daguenet, E., Baguet, A., Degot, S., Schmidt, U., Alpy, F., Wendling, C., Spiegelhalter, C., Kessler, P., Rio, M.-C., Le Hir, H., et al. (2012). Perispeckles are major assembly sites for the exon junction core complex. *Mol. Biol. Cell* *23*, 1765–1782.

Degot, S., Régnier, C.H., Wendling, C., Chenard, M.-P., Rio, M.-C., and Tomasetto, C. (2002). Metastatic Lymph Node 51, a novel nucleo-cytoplasmic protein overexpressed in breast cancer. *Oncogene* *21*, 4422–4434.

Dostie, J., and Dreyfuss, G. (2002). Translation is required to remove Y14 from mRNAs in the cytoplasm. *Curr. Biol.* *12*, 1060–1067.

Duncan, C.D.S., and Mata, J. (2017). Effects of cycloheximide on the interpretation of ribosome profiling experiments in *Schizosaccharomyces pombe*. *Sci. Rep.* *7*, 10331.

van Eeden, F.J., Palacios, I.M., Petronczki, M., Weston, M.J., and St Johnston, D. (2001). Barentsz is essential for the posterior localization of oskar mRNA and colocalizes with it to the posterior pole. *J. Cell Biol.* *154*, 511–523.

Gangras, P., Dayeh, D.M., Mabin, J.W., Nakanishi, K., and Singh, G. (2018). Cloning and Identification of Recombinant Argonaute-Bound Small RNAs Using Next-Generation Sequencing. *Methods Mol. Biol.* *1680*, 1–28.

Gehring, N.H., Kunz, J.B., Neu-Yilik, G., Breit, S., Viegas, M.H., Hentze, M.W., and Kulozik,

A.E. (2005). Exon-junction complex components specify distinct routes of nonsense-mediated mRNA decay with differential cofactor requirements. *Mol. Cell* 20, 65–75.

Gehring, N.H., Lamprinaki, S., Hentze, M.W., and Kulozik, A.E. (2009a). The hierarchy of exon-junction complex assembly by the spliceosome explains key features of mammalian nonsense-mediated mRNA decay. *PLoS Biol.* 7, e1000120.

Gehring, N.H., Lamprinaki, S., Kulozik, A.E., and Hentze, M.W. (2009b). Disassembly of exon junction complexes by PYM. *Cell* 137, 536–548.

Gehring, N.H., Wahle, E., and Fischer, U. (2017). Deciphering the mRNP Code: RNA-Bound Determinants of Post-Transcriptional Gene Regulation. *Trends Biochem. Sci.* 42, 369–382.

Geyer, P.K., Meyuhas, O., Perry, R.P., and Johnson, L.F. (1982). Regulation of ribosomal protein mRNA content and translation in growth-stimulated mouse fibroblasts. *Mol. Cell. Biol.* 2, 685–693.

Halstead, J.M., Lionnet, T., Wilbertz, J.H., Wippich, F., Ephrussi, A., Singer, R.H., and Chao, J.A. (2015). Translation. An RNA biosensor for imaging the first round of translation from single cells to living animals. *Science* 347, 1367–1671.

Hauer, C., Sieber, J., Schwarzl, T., Hollerer, I., Curk, T., Alleaume, A.-M., Hentze, M.W., and Kulozik, A.E. (2016). Exon Junction Complexes Show a Distributional Bias toward Alternatively Spliced mRNAs and against mRNAs Coding for Ribosomal Proteins. *Cell Rep.* 16, 1588–1603.

Hayashi, R., Handler, D., Ish-Horowicz, D., and Brennecke, J. (2014). The exon junction complex is required for definition and excision of neighboring introns in *Drosophila*. *Genes Dev.* 28, 1772–1785.

Haynes, C., and Iakoucheva, L.M. (2006). Serine/arginine-rich splicing factors belong to a class of intrinsically disordered proteins. *Nucleic Acids Res.* 34, 305–312.

Hentze, M.W., Castello, A., Schwarzl, T., and Preiss, T. (2018). A brave new world of RNA-binding proteins. *Nat. Rev. Mol. Cell Biol.* 19, 327–341.

Huang, D.W., Sherman, B.T., and Lempicki, R.A. (2009). Systematic and integrative analysis of large gene lists using DAVID bioinformatics resources. *Nat. Protoc.* 4, 44–57.

Ingolia, N.T., Lareau, L.F., and Weissman, J.S. (2011). Ribosome profiling of mouse embryonic

stem cells reveals the complexity and dynamics of mammalian proteomes. *Cell* 147, 789–802.

Jan, C.H., Williams, C.C., and Weissman, J.S. (2014). Principles of ER cotranslational translocation revealed by proximity-specific ribosome profiling. *Science* 346, 1257521.

Kiss, D.L., Baez, W., Huebner, K., Bundschuh, R., and Schoenberg, D.R. (2017). Impact of FHIT loss on the translation of cancer-associated mRNAs. *Mol. Cancer* 16, 179.

Kwon, I., Xiang, S., Kato, M., Wu, L., Theodoropoulos, P., Wang, T., Kim, J., Yun, J., Xie, Y., and McKnight, S.L. (2014). Poly-dipeptides encoded by the C9orf72 repeats bind nucleoli, impede RNA biogenesis, and kill cells. *Science* 345, 1139–1145.

Lee, S.R., and Lykke-Andersen, J. (2013). Emerging roles for ribonucleoprotein modification and remodeling in controlling RNA fate. *Trends Cell Biol.* 23, 504–510.

Le Hir, H., Saulière, J., and Wang, Z. (2016). The exon junction complex as a node of post-transcriptional networks. *Nat. Rev. Mol. Cell Biol.* 17, 41–54.

Love, M.I., Huber, W., and Anders, S. (2014). Moderated estimation of fold change and dispersion for RNA-seq data with DESeq2. *Genome Biol.* 15, 550.

Lykke-Andersen, J., Shu, M.D., and Steitz, J.A. (2001). Communication of the position of exon-exon junctions to the mRNA surveillance machinery by the protein RNPS1. *Science* 293, 1836–1839.

Macchi, P., Kroening, S., Palacios, I.M., Baldassa, S., Grunewald, B., Ambrosino, C., Goetze, B., Lupas, A., St Johnston, D., and Kiebler, M. (2003). Barentsz, a new component of the Staufen-containing ribonucleoprotein particles in mammalian cells, interacts with Staufen in an RNA-dependent manner. *J. Neurosci.* 23, 5778–5788.

Malone, C.D., Mestdagh, C., Akhtar, J., Kreim, N., Deinhard, P., Sachidanandam, R., Treisman, J., and Roignant, J.-Y. (2014). The exon junction complex controls transposable element activity by ensuring faithful splicing of the piwi transcript. *Genes Dev.* 28, 1786–1799.

Mao, H., Brown, H.E., and Silver, D.L. (2017). Mouse models of Casc3 reveal developmental functions distinct from other components of the exon junction complex. *RNA* 23, 23–31.

Meyuhas, O., and Kahan, T. (2015). The race to decipher the top secrets of TOP mRNAs. *Biochim. Biophys. Acta* 1849, 801–811.

Murachelli, A.G., Ebert, J., Basquin, C., Le Hir, H., and Conti, E. (2012). The structure of the ASAP core complex reveals the existence of a Pinin-containing PSAP complex. *Nat. Struct. Mol. Biol.* *19*, 378–386.

Neve, J., Burger, K., Li, W., Hoque, M., Patel, R., Tian, B., Gullerova, M., and Furger, A. (2016). Subcellular RNA profiling links splicing and nuclear DICER1 to alternative cleavage and polyadenylation. *Genome Res.* *26*, 24–35.

Pandit, S., Zhou, Y., Shiue, L., Coutinho-Mansfield, G., Li, H., Qiu, J., Huang, J., Yeo, G.W., Ares, M., Jr, and Fu, X.-D. (2013). Genome-wide analysis reveals SR protein cooperation and competition in regulated splicing. *Mol. Cell* *50*, 223–235.

Paradis, C., Cloutier, P., Shkreta, L., Toutant, J., Klarskov, K., and Chabot, B. (2007). hnRNP I/PTB can antagonize the splicing repressor activity of SRp30c. *RNA* *13*, 1287–1300.

Patursky-Polischuk, I., Stolovich-Rain, M., Hausner-Hanochi, M., Kasir, J., Cybulski, N., Avruch, J., Rüegg, M.A., Hall, M.N., and Meyuhass, O. (2009). The TSC-mTOR pathway mediates translational activation of TOP mRNAs by insulin largely in a raptor- or rictor-independent manner. *Mol. Cell. Biol.* *29*, 640–649.

Quinlan, A.R., and Hall, I.M. (2010). BEDTools: a flexible suite of utilities for comparing genomic features. *Bioinformatics* *26*, 841–842.

Ray, D., Kazan, H., Cook, K.B., Weirauch, M.T., Najafabadi, H.S., Li, X., Gueroussov, S., Albu, M., Zheng, H., Yang, A., et al. (2013). A compendium of RNA-binding motifs for decoding gene regulation. *Nature* *499*, 172–177.

Roignant, J.-Y., and Treisman, J.E. (2010). Exon junction complex subunits are required to splice *Drosophila* MAP kinase, a large heterochromatic gene. *Cell* *143*, 238–250.

Sato, H., Hosoda, N., and Maquat, L.E. (2008). Efficiency of the pioneer round of translation affects the cellular site of nonsense-mediated mRNA decay. *Mol. Cell* *29*, 255–262.

Saulière, J., Murigneux, V., Wang, Z., Marquet, E., Barbosa, I., Le Tonquèze, O., Audic, Y., Paillard, L., Roest Crolius, H., and Le Hir, H. (2012). CLIP-seq of eIF4AIII reveals transcriptome-wide mapping of the human exon junction complex. *Nat. Struct. Mol. Biol.* *19*, 1124–1131.

- Schwanhäusser, B., Busse, D., Li, N., Dittmar, G., Schuchhardt, J., Wolf, J., Chen, W., and Selbach, M. (2011). Global quantification of mammalian gene expression control. *Nature* *473*, 337–342.
- Singh, G., Jakob, S., Kleedehn, M.G., and Lykke-Andersen, J. (2007). Communication with the exon-junction complex and activation of nonsense-mediated decay by human Upf proteins occur in the cytoplasm. *Mol. Cell* *27*, 780–792.
- Singh, G., Kucukural, A., Cenik, C., Leszyk, J.D., Shaffer, S.A., Weng, Z., and Moore, M.J. (2012). The cellular EJC interactome reveals higher-order mRNP structure and an EJC-SR protein nexus. *Cell* *151*, 750–764.
- Singh, G., Ricci, E.P., and Moore, M.J. (2014). RIPiT-Seq: a high-throughput approach for footprinting RNA:protein complexes. *Methods* *65*, 320–332.
- Singh, G., Pratt, G., Yeo, G.W., and Moore, M.J. (2015). The Clothes Make the mRNA: Past and Present Trends in mRNP Fashion. *Annu. Rev. Biochem.* *84*, 325–354.
- Tacke, R., and Manley, J.L. (1995). The human splicing factors ASF/SF2 and SC35 possess distinct, functionally significant RNA binding specificities. *EMBO J.* *14*, 3540–3551.
- Tacke, R., Tohyama, M., Ogawa, S., and Manley, J.L. (1998). Human Tra2 proteins are sequence-specific activators of pre-mRNA splicing. *Cell* *93*, 139–148.
- Tange, T.Ø., Shibuya, T., Jurica, M.S., and Moore, M.J. (2005). Biochemical analysis of the EJC reveals two new factors and a stable tetrameric protein core. *RNA* *11*, 1869–1883.
- Tani, H., Mizutani, R., Salam, K.A., Tano, K., Ijiri, K., Wakamatsu, A., Isogai, T., Suzuki, Y., and Akimitsu, N. (2012). Genome-wide determination of RNA stability reveals hundreds of short-lived noncoding transcripts in mammals. *Genome Res.* *22*, 947–956.
- Trapnell, C., Pachter, L., and Salzberg, S.L. (2009). TopHat: discovering splice junctions with RNA-Seq. *Bioinformatics* *25*, 1105–1111.
- Trcek, T., Sato, H., Singer, R.H., and Maquat, L.E. (2013). Temporal and spatial characterization of nonsense-mediated mRNA decay. *Genes Dev.* *27*, 541–551.
- Viegas, M.H., Gehring, N.H., Breit, S., Hentze, M.W., and Kulozik, A.E. (2007). The abundance of RNPS1, a protein component of the exon junction complex, can determine the variability in

efficiency of the Nonsense Mediated Decay pathway. *Nucleic Acids Res.* 35, 4542–4551.

Walter, P., and Blobel, G. (1981). Translocation of proteins across the endoplasmic reticulum III. Signal recognition protein (SRP) causes signal sequence-dependent and site-specific arrest of chain elongation that is released by microsomal membranes. *J. Cell Biol.* 91, 557–561.

Woodward, L.A., Mabin, J.W., Gangras, P., and Singh, G. (2017). The exon junction complex: a lifelong guardian of mRNA fate. *Wiley Interdiscip. Rev. RNA* 8.

Zhang, Z., and Krainer, A.R. (2004). Involvement of SR proteins in mRNA surveillance. *Mol. Cell* 16, 597–607.

Zhang, X., Yan, C., Hang, J., Finci, L.I., Lei, J., and Shi, Y. (2017). An Atomic Structure of the Human Spliceosome. *Cell* 169, 918–929.e14.

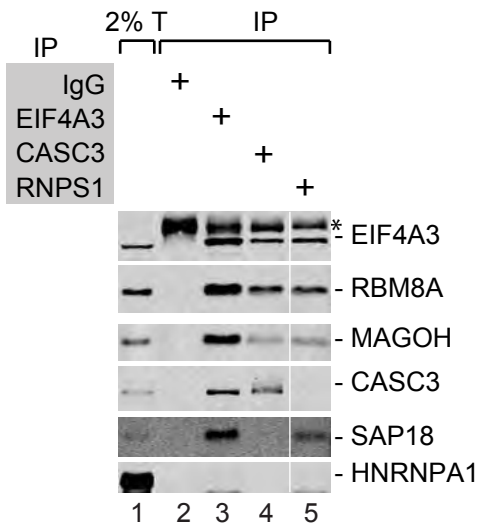
Zhang, Y., Wen, Z., Washburn, M.P., and Florens, L. (2010). Refinements to label free proteome quantitation: how to deal with peptides shared by multiple proteins. *Anal. Chem.* 82, 2272–2281.

Zhong, X.-Y., Wang, P., Han, J., Rosenfeld, M.G., and Fu, X.-D. (2009). SR proteins in vertical integration of gene expression from transcription to RNA processing to translation. *Mol. Cell* 35, 1–10.

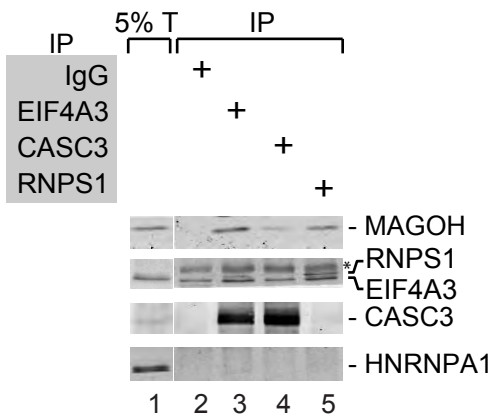
Zhou, Z., and Fu, X.-D. (2013). Regulation of splicing by SR proteins and SR protein-specific kinases. *Chromosoma* 122, 191–207.

Figure 1

A



B



C

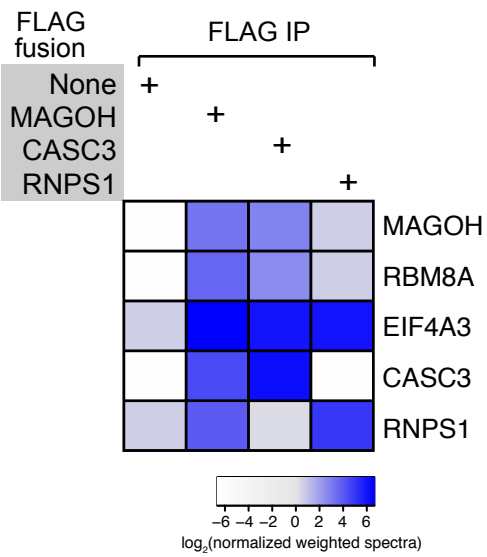


Figure 1. RNPS1 and CASC3 exists in mutually exclusive EJC in mammalian cells.

(A) Alternate EJCs in HEK293 cells. Western blots showing proteins on the right in total cell extract (T) (lane 1) or the immuno-precipitates (IP) (lanes 2-5) of the antibodies listed on the top. The asterisk (*) indicates signal from IgG heavy chain.

(B) Alternate EJCs in mouse cortical total extracts and IPs as in (A).

(C) Confirmation of mutually exclusive interactions via bottom-up proteomics. Heatmap showing signal for normalized-weighted spectra observed for the proteins on the right in the indicated FLAG IPs (top). The color scale for \log_2 transformed normalized-weighted spectral values is shown below.

Figure 2

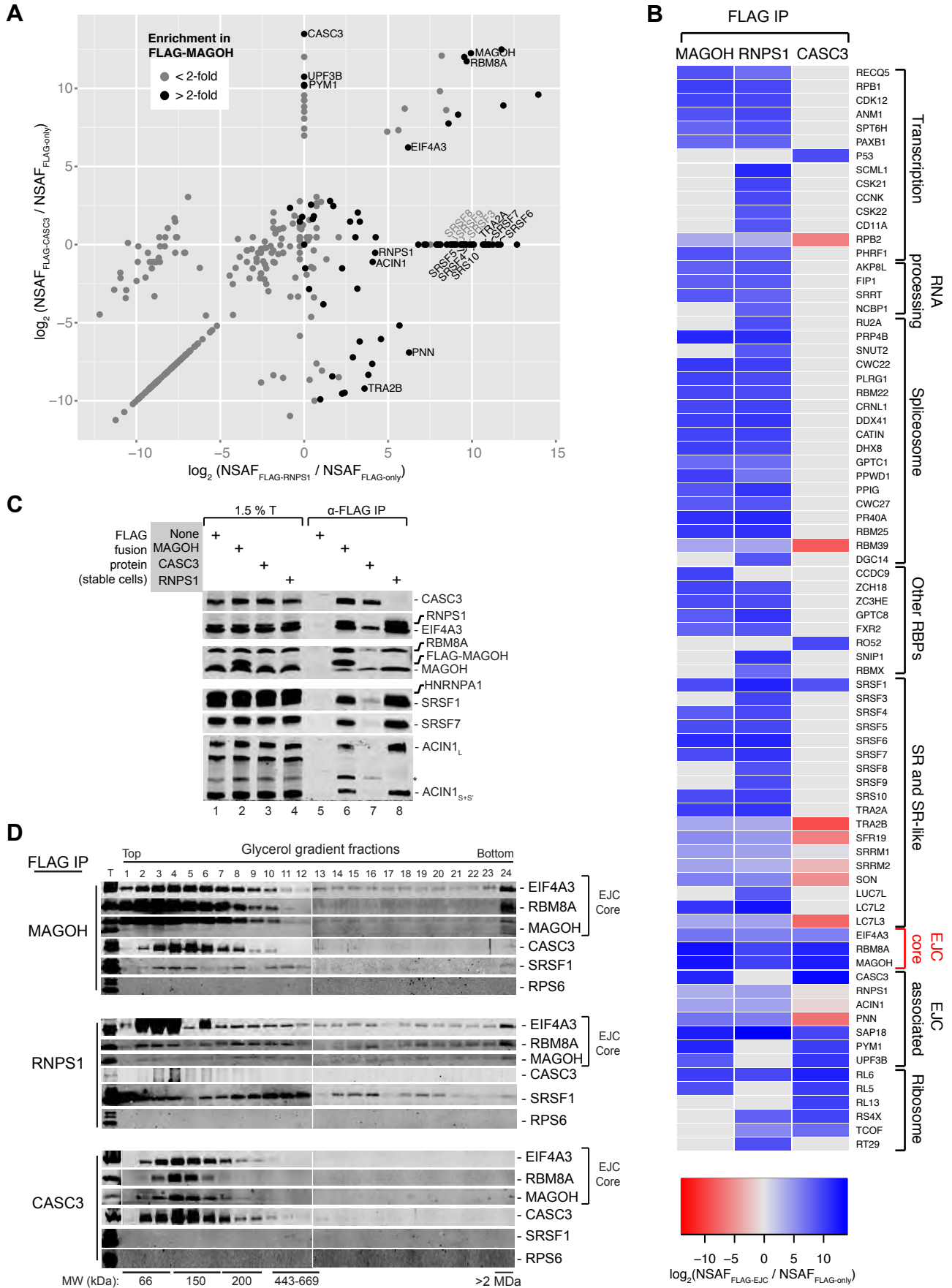


Figure 2. CASC3- and RNPS1-containing complexes have distinct protein composition and hydrodynamic size.

- (A) Comparison of alternate EJC proteomes-I. A scatter plot where \log_2 transformed values are compared for fold-enrichment of proteins in FLAG-RNPS1 IP over FLAG-only control (x-axis) to fold-enrichment of the same proteins in FLAG-CASC3 IP over FLAG-only control (y-axis). Protein quantification was performed using Normalized Spectral Abundance Factor (NSAF). Each dot represents a protein that was identified in FLAG-EJC or FLAG-only control samples by Scaffold (see experimental procedures). Black dots: proteins enriched >2-fold over control in the FLAG-Magoh IP.
- (B) Comparison of alternate EJC proteomes-II. A heatmap showing proteins that are >10-fold enriched in any of the FLAG-EJC IPs (indicated on the top) over FLAG-only control (proteins deemed to be contaminants were omitted). Proteins are grouped according to common functions (right). The color scale for the heatmap is at the bottom.
- (C) Validation of mass spec. Western blots showing proteins (right) in total extract (T) or FLAG-IPs as on the top from HEK293 cells stably expressing FLAG-tagged proteins indicated on the top left. Note that RNPS1 migrates just above EIF4A3. The asterisk (*) indicates cross-reaction with CASC3 observed with anti-ACIN1 antibody.
- (D) Hydrodynamic sizes of the alternate EJCs. Western blots showing proteins on the right in glycerol gradient fractions of FLAG-IPs from HEK293 cells stably expressing FLAG-MAGOH, FLAG-RNPS1, or FLAG-CASC3 (far left). The position of fractions from gradients (top) and molecular weight standards are indicated (bottom).

Figure 3

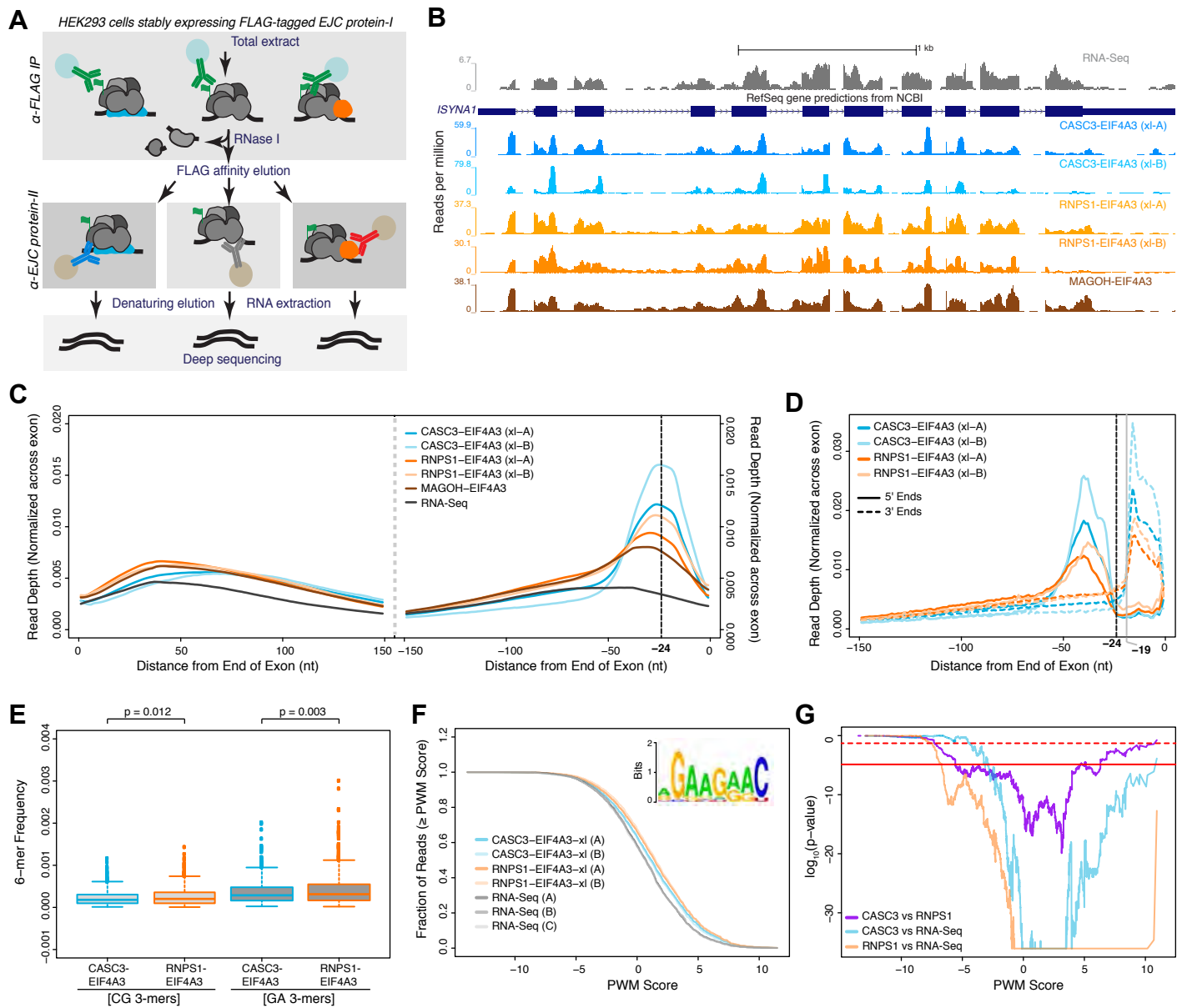
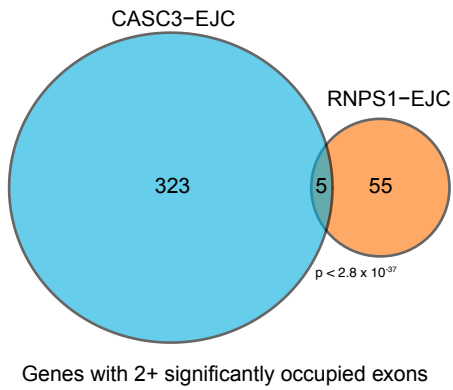


Figure 3. RNPS1 assembles with canonical and non-canonical EJs but CASC3 is mainly part of canonical EJs.

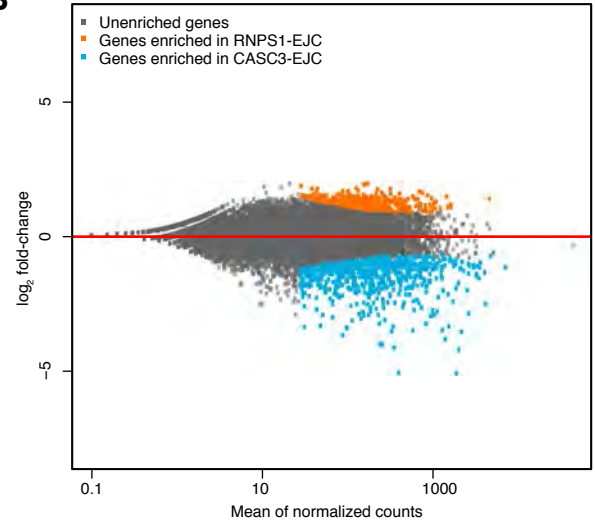
- (A) A schematic illustrating main steps in RNA:protein Immunoprecipitation in Tandem (RIPiT)-Seq.
- (B) Genome browser screen-shots comparing read coverage along the *ISYNA1* gene in RNA-Seq or RIPiT-Seq libraries (indicated on the right). The y-axis of each track in this window was normalized to millions of reads in each library. Blue rectangles: exons; thinner rectangles: untranslated regions; lines with arrows: introns.
- (C) Meta-exon plots showing read depth in different RIPiT-Seq or RNA-Seq libraries (indicated in the middle) in the 150 nucleotides (nt) from the exon 5' end (left) or from the exon 3' end (right). The vertical black dotted line marks the -24 nt position previously determined to be the site of canonical EJs (Singh et al., 2012).
- (D) A composite plot of RNPS1 and CASC3 RIPiT-Seq footprint read 5' (solid lines) and 3' (dotted lines) ends. The canonical EJC site (-24 nt) is indicated by the vertical dotted line. Note there is some variability in the 5' boundary of EJs whereas the 3' boundary is more strict (indicated by the vertical grey line at the -19 position).
- (E) Box plots showing frequencies of 6-mers that contained CG 3-mers (CGG, GCG, CCG, CGC) or GA 3-mers (GGA, GAA, AGG, GAG) in CASC3 or RNPS1 RIPiT-Seq reads. Top: p-values based on Wilcoxon rank-sum test.
- (F) Cumulative distribution function plots showing frequency of reads in the indicated samples with the highest score for match to SRSF1 motif (inset) position weight matrix (PWM). Sample identity is in the legend on the bottom left. The SRSF1 motif shown in the inset is from (Tacke and Manley, 1995).
- (G) A negative binomial based assessment of significance of differences in SRSF1 motif PWM scores in (F) between the two alternate EJC footprint reads or between alternate EJC and RNA-Seq reads (legend on the bottom left). The horizontal dotted red line indicates $p=0.05$ whereas the horizontal solid red line indicates the Bonferroni adjusted p-value.

Figure 4

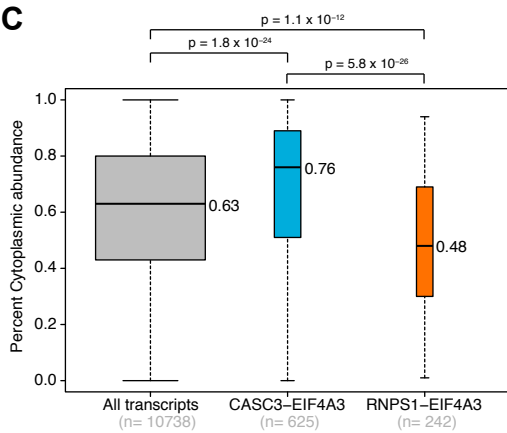
A



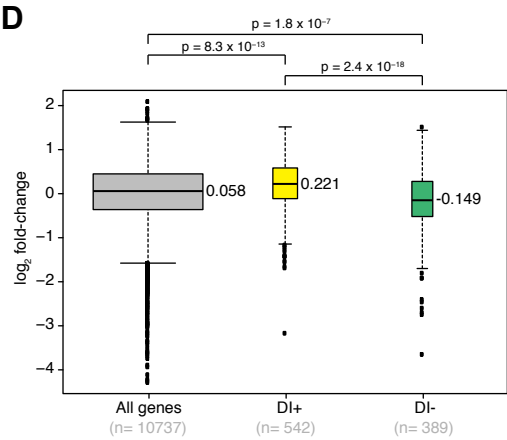
B



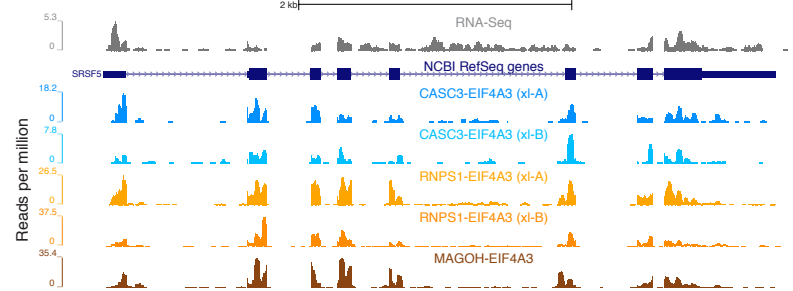
C



D



E



F

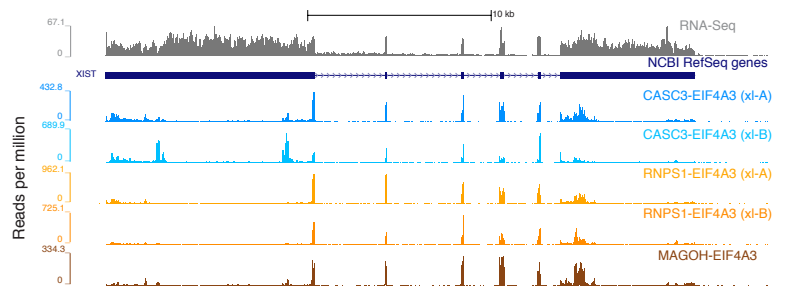


Figure 4. RNPS1 and CASC3 occupy same RNAs and sites but in different subcellular compartments.

- (A) A venn-diagram showing genes with at least two differentially enriched exons, for which all differentially enriched exons are preferentially bound to CASC3-EJC (blue region), RNPS1-EJC (orange region), or genes with at least one exon is enriched in CASC3-EJC and one in RNPS1-EJC (overlap region). ($p < 2.8 \times 10^{-37}$). p-value shown was obtained as the probability of observing an overlap of 5 or fewer genes using a binomial distribution approximating each gene as containing two exons.
- (B) An MA-plot showing fold-change in RNPS1-EJC versus CASC3-EJC footprint reads (y-axis) against expression levels (x-axis). Each dot represents a canonical transcript for each known gene in GRCh38 from UCSC “knownCanonical” splice variant table. Transcripts determined to be differentially enriched (p -adjusted <0.05) in RNPS1-EJC (orange) and CASC3-EJC (blue) are indicated.
- (C) Box plots showing distribution of percent cytoplasmic levels (y-axis) for all (grey), CASC3-EJC enriched (blue), and RNPS1-EJC enriched (orange) transcripts. The median values are given to the right of each box plot. p-values on the top are based on Wilcoxon rank sum test. Bottom: The number of transcripts in each group.
- (D) Box plots showing distribution of fold-change values (y-axis) for RNPS1-EJC versus CASC3-EJC footprint read counts for all (grey), detained intron-containing (DI+; yellow) or detained intron-lacking (DI-; green) transcripts. (+ve values: enriched in RNPS1-EJC; -ve values: enriched in CASC3-EJC). Top: p-values (Wilcoxon rank sum test). Bottom: the number of transcripts in each group.
- (E) Genome browser screen-shots showing read coverage along the *SRSF5* gene in RNA-Seq (top) or RIPiT-Seq libraries (labeled on right). Blue rectangles: exons; thinner rectangles: untranslated regions; lines with arrows: introns. Note increased RNA-Seq reads in introns 4 and 5.
- (F) Genome browser screen-shot as in (E) for the *XIST* locus.

Figure 5

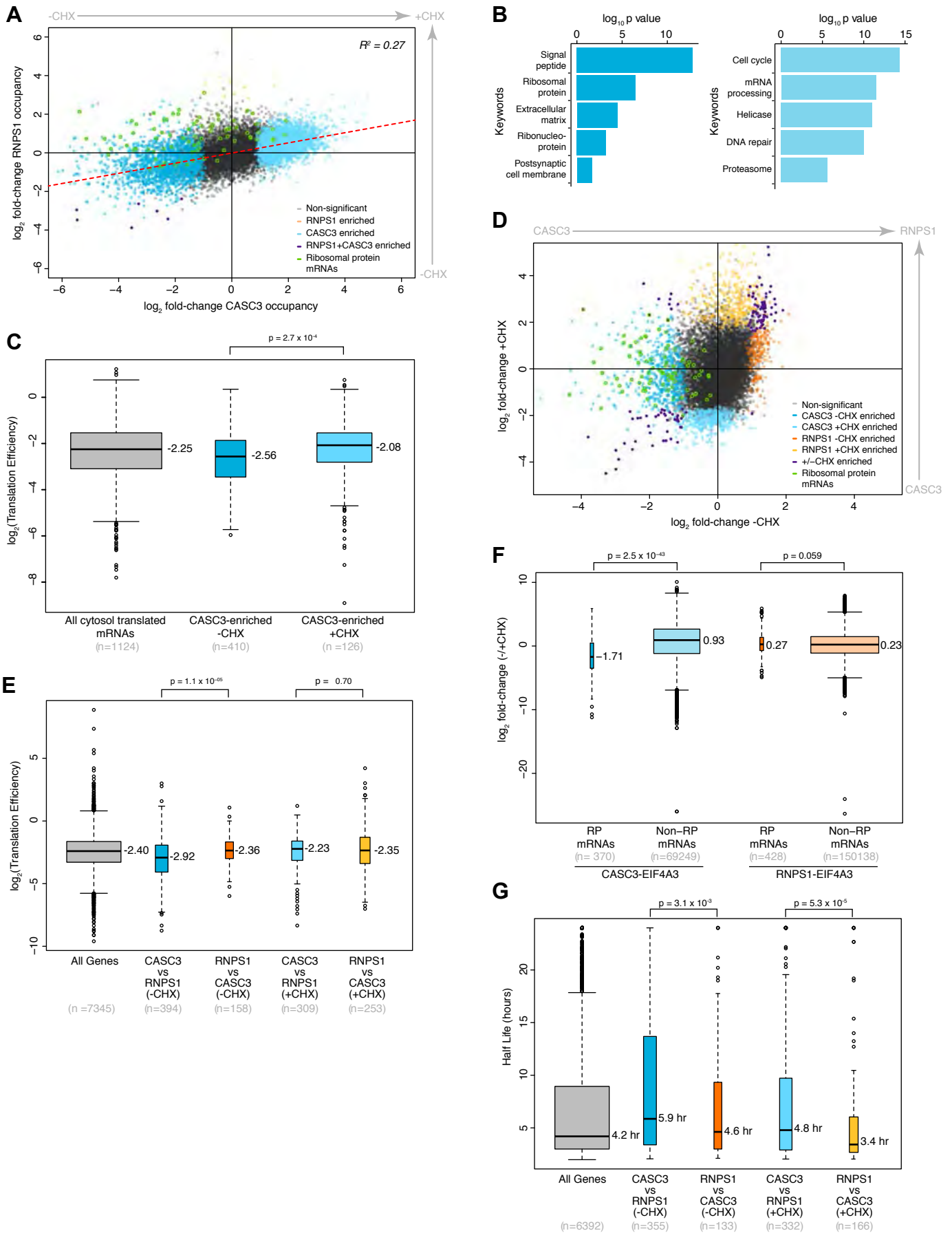


Figure 5. Translation and mRNA decay kinetics impacts alternate EJC occupancy.

- (A) A scatter plot showing fold-change in CASC3-EJC occupancy in absence versus presence of cycloheximide (CHX; x-axis) and fold-change in RNPS1-EJC in absence versus presence of CHX (y-axis). Each dot represents a canonical transcript for each known gene in GRChg38, and is colored as indicated in the legend (bottom right). The dots representing ribosomal protein genes are highlighted by a green outline. The dotted red line shows a linear fit and the coefficient of determination (R^2) is on the top left corner.
- (B) Top 5 GO term keywords and their \log_{10} transformed p-values of enrichment in CASC3-EJC enriched transcripts (from A) in the absence (left) or presence of CHX (right).
- (C) Box plots showing distribution of translation efficiency estimates (y-axis) of transcript groups on y-axis. The median values are given to the right of each box plot. Top: p-values (Wilcoxon rank sum test). Bottom: the number of transcripts in each group.
- (D) Scatter plot as in (A) comparing fold-change in CASC3-EJC versus RNPS1-EJC footprint read counts in -CHX (x-axis) and +CHX (y-axis) conditions.
- (E) Box plots as in (C) showing distribution of translation efficiency estimates of transcript groups from (D) as indicated on the bottom.
- (F) Comparison of fold-change in CASC3-EJC or RNPS1-EJC footprint reads at canonical EJC sites (as defined in the methods section) from ribosomal protein (RP)-coding mRNAs or non-ribosomal (non-RP)-protein coding mRNAs. Top: p-values (Wilcoxon rank sum test).
- (G) Box plots as in (C) and (E) above comparing mRNA half-life of transcript groups from (D) as indicated on the bottom.

Figure 6

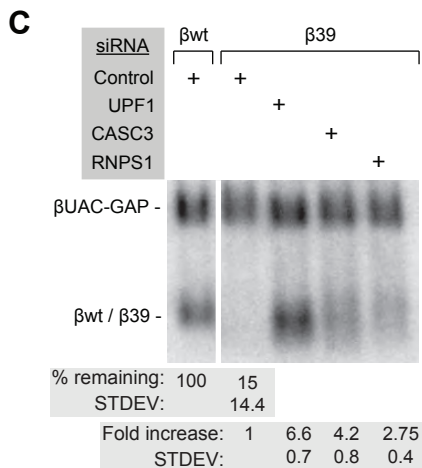
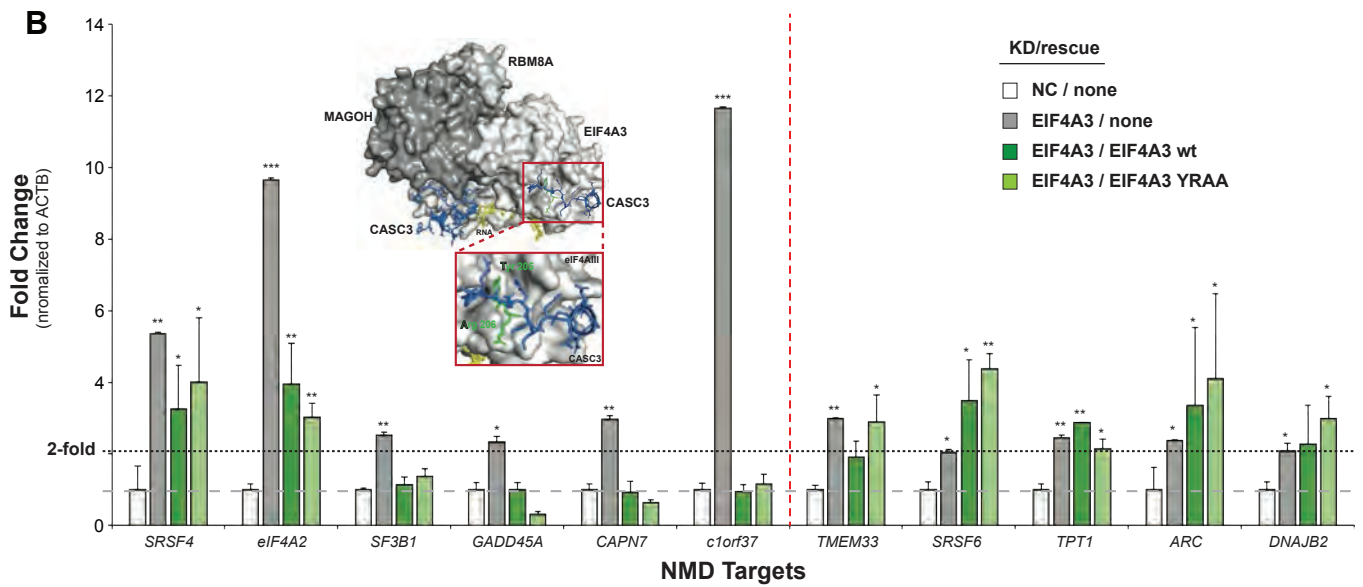
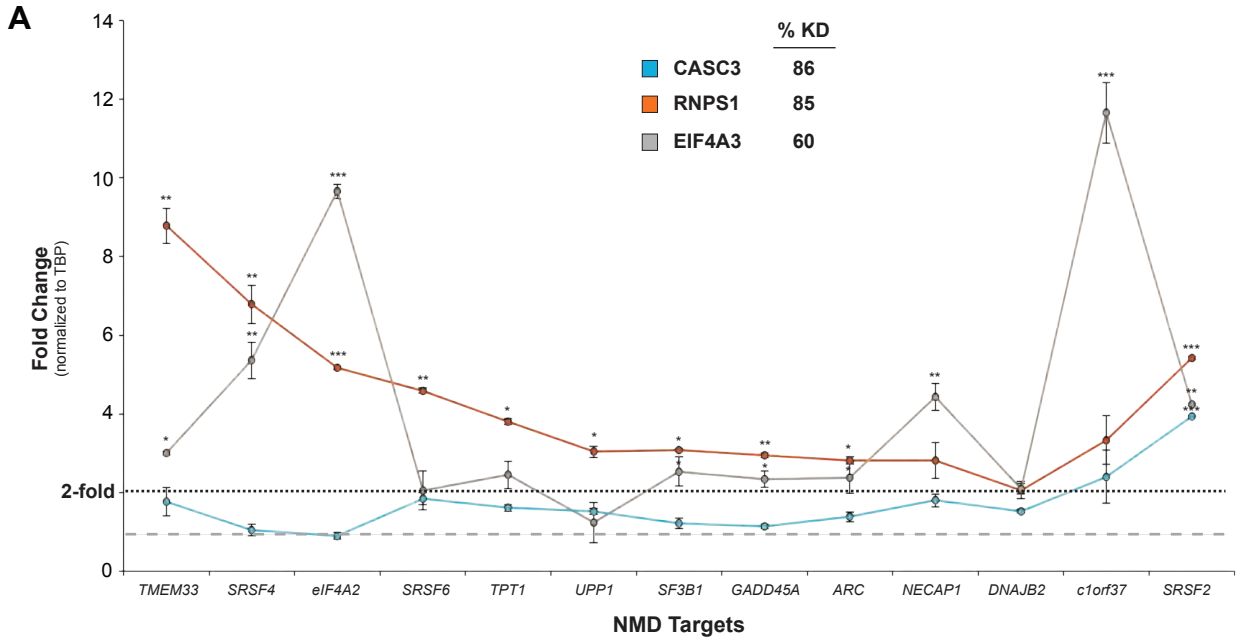


Figure 6. RNPS1 is required whereas CASC3 is largely dispensable for efficient NMD.

(A) Fold change as measured by real-time PCR in abundance of endogenous NMD-targeted transcripts (bottom) in HEK293 cells depleted of core or alternate EJC factors. (EIF4A3 knockdown: 48 hr, alternate EJC factor knockdown: 96 hr). Shown are the average values normalized to TBP levels from three biological replicates \pm standard error of means (SEM). Asterisks denote statistically significant differences: * $p < 0.05$, ** $p < 0.01$, *** $p < 0.001$ (Welch's t-test). Percent knockdown of each protein in a representative experiment is in the legend (see Figure S6).

(B) Real-time PCR analysis as in (A) from HEK293 cells depleted of EIF4A3. Either wild-type EIF4A3 or a mutant lacking CASC3 interaction were exogenously expressed in EIF4A3 knockdown cells as indicated in the legend on the top right. Inset: An EJC core crystal structure (PDB ID: 2J0S) showing the EIF4A3 residues that interact with CASC3 (enlarged below). The vertical red dotted line divides the NMD targets into two groups based on the degree of NMD restoration.

(C) Northern blots showing levels of wild-type (β wt, lane 1) or PTC-containing (codon 39; β 39; lanes 2-5) β -globin mRNA and a longer internal control β -globin (β UAC-GAP) mRNA from HeLa Tet-off cells treated with siRNAs indicated on the top. Tables below indicate percentage of normalized β 39 mRNA as compared to normalized β wt mRNA (top) or fold-increase in β 39 mRNA upon knockdown as compared to control.

Figure 7

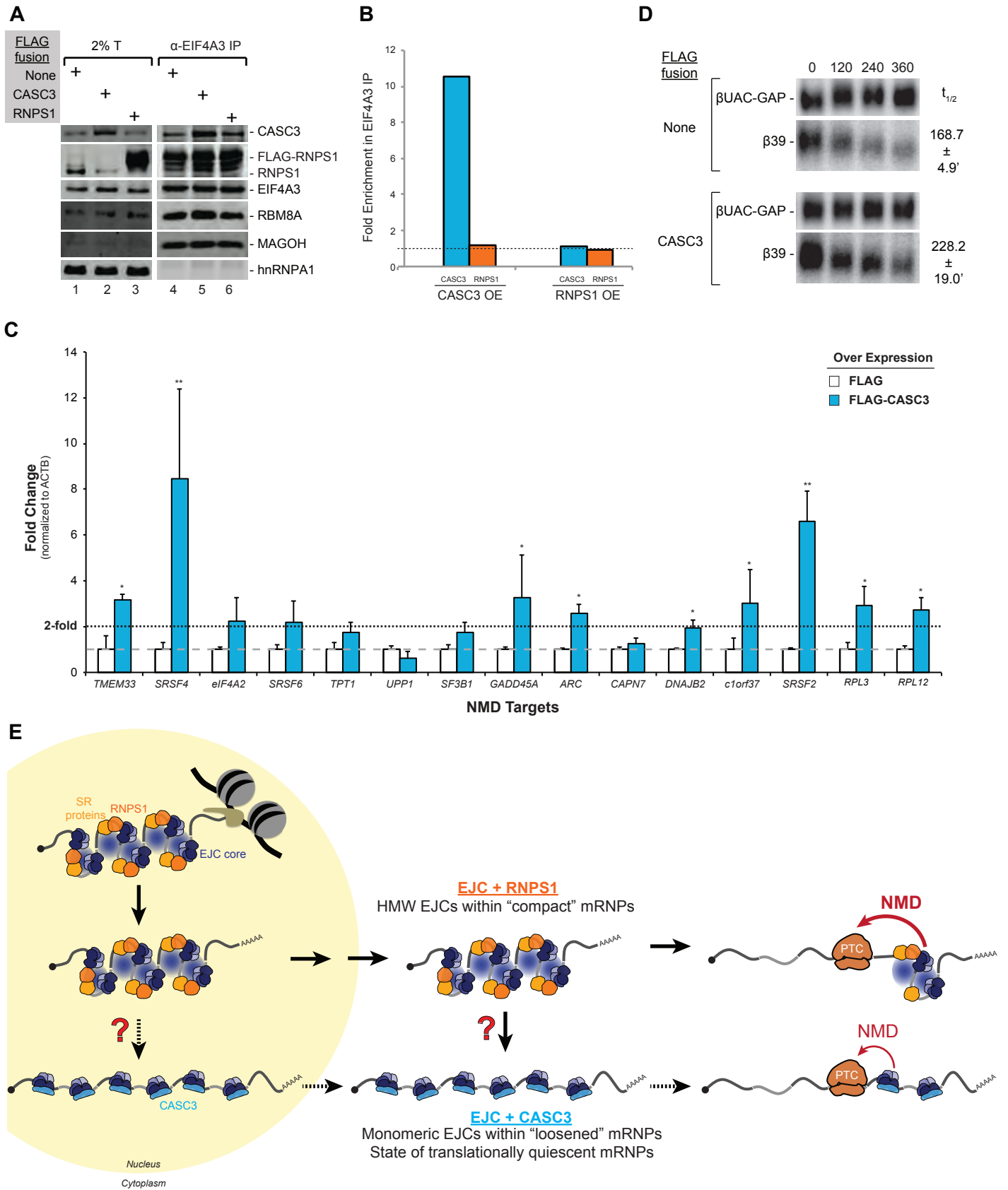
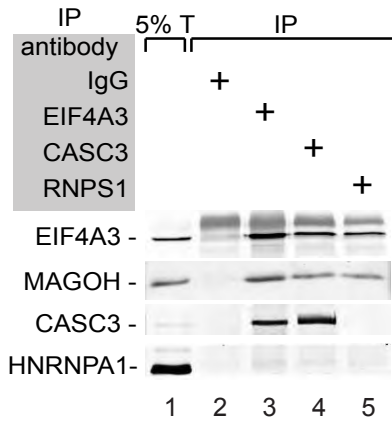


Figure 7. Promotion of switch to late-acting CASC3-EJC dampens NMD activity.

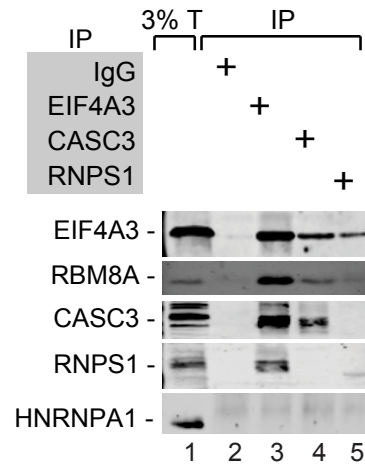
- (A) Western blots showing proteins on the right in total extract (T, lanes 1-3) or EIF4AIII IPs (lanes 4-6) from HEK293 cells overexpressing FLAG-fusion proteins at top left.
- (B) Histogram showing the fold enrichment of alternate EJC factors in EIF4A3 IPs from (A). Overexpressed (OE) alternate EJC factors are at the bottom and CASC3 (blue) and RNPS1 (orange) levels in each OE sample (lane 5 or 6) were compared to the control IP in lane 4 (grey, set to 1).
- (C) Fold change in abundance of NMD-targeted endogenous transcripts (bottom) in HEK293 cells exogenously overexpressing FLAG or FLAG-CASC3. Shown are the average values normalized to ACTB levels from three biological replicates \pm SEM. Asterisks denote statistically significant differences: * $p < 0.05$, ** $p < 0.01$, *** $p < 0.001$ (Welch's t-test).
- (D) Northern blots showing decay of Tetracycline-inducible $\beta 39$ mRNA as compared to constitutively expressed β UAC-GAP mRNA in HeLa Tet-off cells overexpressing FLAG-tagged proteins indicated on the left. Time after Tet-mediated transcriptional shut-off of $\beta 39$ mRNA is indicated on the top. On the right is $\beta 39$ mRNA half-life ($t_{1/2}$) from each condition (average of three biological replicates \pm standard deviation).
- (E) A model depicting switch in EJC composition and its effect on mRNP structure and NMD activity. Key EJC proteins are indicated. Oval with radial blue fill in the high molecular weight (HMW) EJCs represent unknown interactions that mediate EJC multimerization. Grey and black lines: exons.

Figure S1

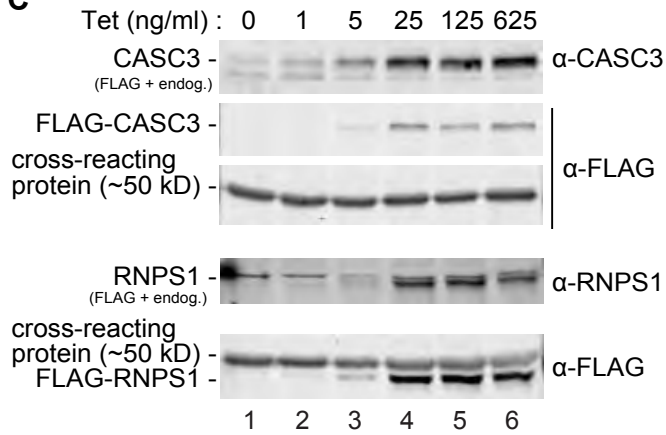
A



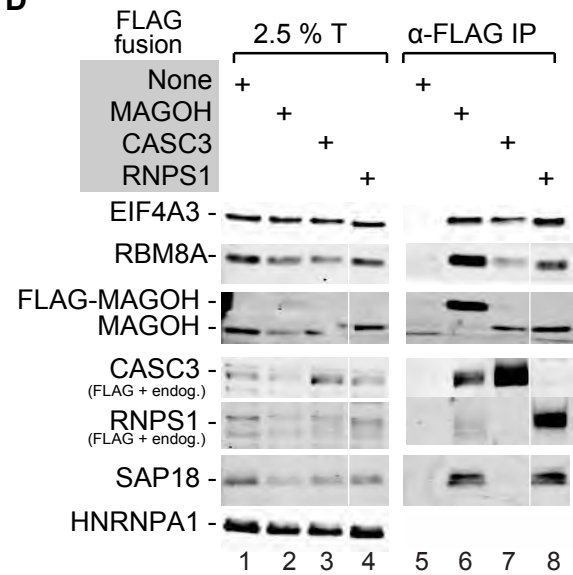
B



C



D



E

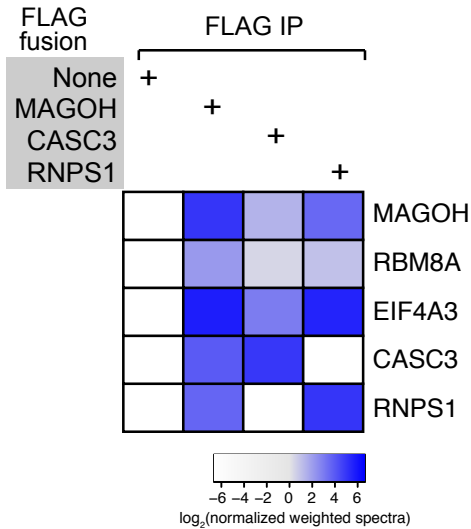


Figure S1. (related to Figure 1)

- (A) Alternate EJCs in P19 cells. Western blots showing proteins on the left in P19 total cell extract (T, lane 1) or the immuno-precipitates (IP, lanes 2-5) using the antibodies listed on the top.
- (B) Alternate EJCs in HeLa cells as in (A).
- (C) Tetracycline (Tet)-induction of FLAG-tagged CASC3 and RNPS1. Western blots showing Tet-induced expression of FLAG-fusion proteins in FLP-In TREx Tet-on HEK293 cell lines. Tet concentrations are on the top, proteins detected are on the left and antibodies used for westerns are on the right.
- (D) Tagged proteins assemble into alternate EJCs. Western blots showing proteins on the left in TE or FLAG IPs of FLAG-fusion proteins expressed in HEK293 cells at near-endogenous levels.
- (E) Alternate EJC proteomic analysis (replicate 2). Heatmap showing enrichment of proteins on the right in FLAG-EJC protein IP proteomic analysis (indicated on the top).

Figure S2

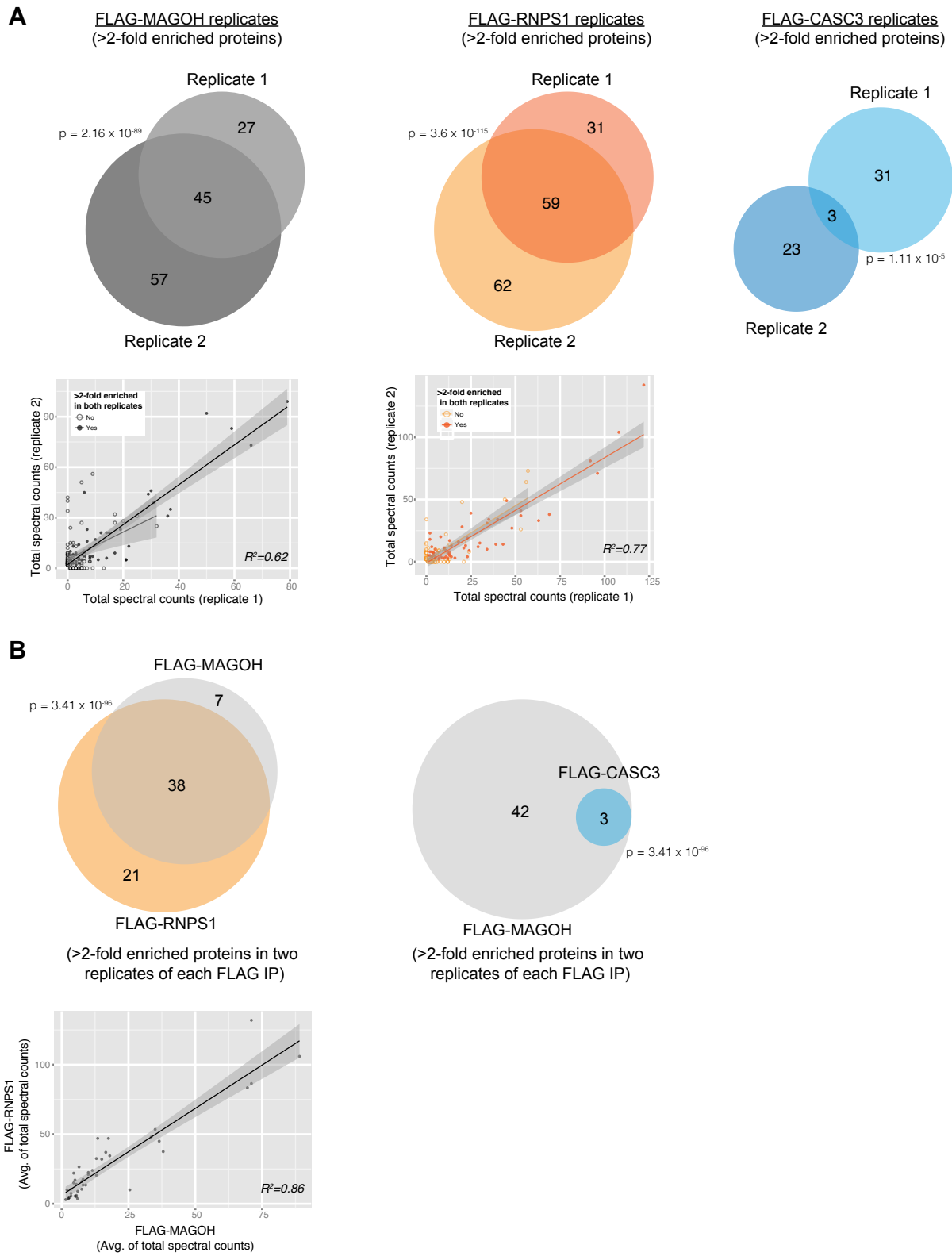


Figure S2. (related to Figure 2)

- (A) Comparison between the two biological replicates of each FLAG-EJC mass spec samples. Overlap between >2-fold enriched proteins in the two biological replicates of proteomics samples of FLAG-EJC proteins indicated on the top. Hypergeometric test p-values are shown next to each venn diagram. For FLAG-MAGOH and FLAG-RNPS1 replicates, scatter plots compare total spectral counts for proteins detected in the two biological replicates. The linear fits for proteins enriched less or more than 2-fold are shown as indicated in the legend. Spearman correlation coefficient for >2-fold enriched proteins in each sample is shown.
- (B) Comparisons as in (A) between the reproducibly enriched proteins in FLAG-MAGOH with those enriched in both replicates of FLAG-RNPS1 (left) and FLAG-CASC3 (right).

Figure S3

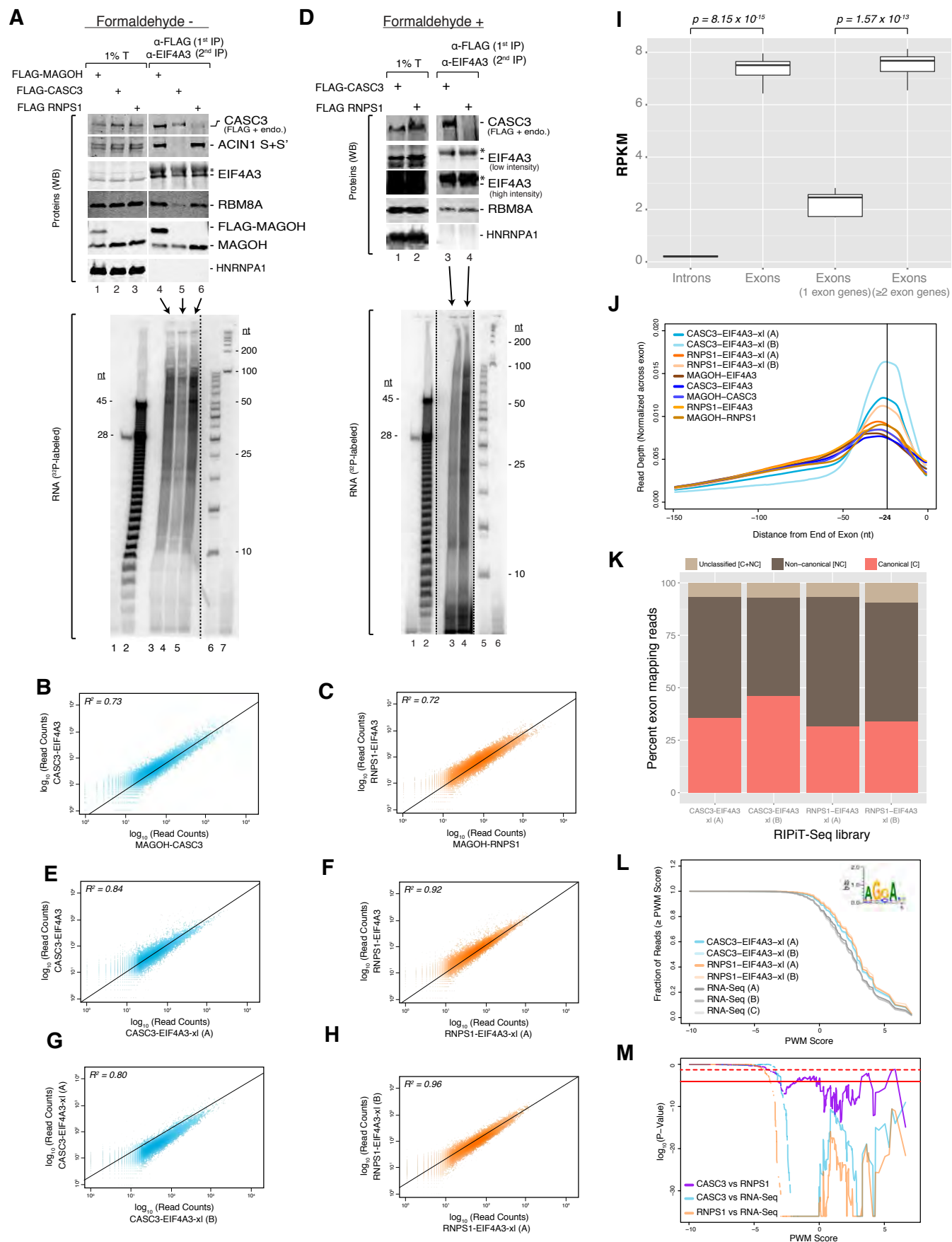


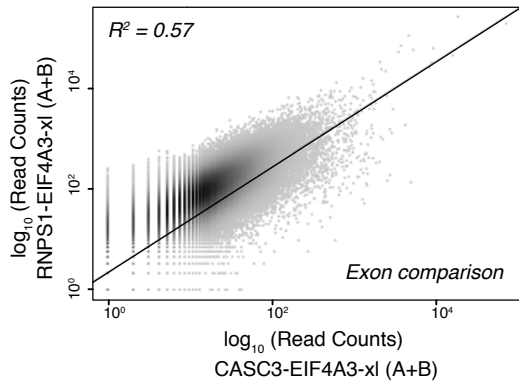
Figure S3. (related to Figure 3)

- (A) Proteins and RNAs enriched in native alternate EJC RIPiTs. Top: Western blots with proteins indicated on the right in TE or RIPiT elutions. Bottom: Autoradiogram of end labeled RNAs from RIPiT elutions as well as size-markers (indicated on either side). The asterisk (*) indicates detection of IgG heavy chain.
- (B) Comparison between native CASC3-EJC RIPiT-Seq samples [FLAG-MAGOH:CASC3 (x-axis) versus FLAG-CASC3:EIF4A3 (y-axis)]. Scatter plot comparing read counts for canonical transcripts for each known gene in GRChg38 (represented by each dot). A linear fit and Spearman correlation coefficient are also shown.
- (C) Comparison between native RNPS1-EJC RIPiT-Seq samples [FLAG-MAGOH:RNPS1 (x-axis) versus FLAG-RNPS1:EIF4A3 (y-axis)] as in (C).
- (D) Proteins and RNAs enriched in formaldehyde-crosslinked alternate EJC RIPiTs as in (A).
- (E) Comparison as in (C) between native and formaldehyde-crosslinked CASC3-EJC RIPiT-Seq samples [FLAG-CASC3:EIF4A3, formaldehyde-crosslinked (xl), replicate A (x-axis) versus native FLAG-CASC3:EIF4A3 (y-axis)].
- (F) Comparison as in (C) between native and formaldehyde-crosslinked RNPS1-EJC RIPiT-Seq samples [FLAG-RNPS1:EIF4A3, formaldehyde-crosslinked (xl), replicate A (x-axis) versus native FLAG-RNPS1:EIF4A3 (y-axis)].
- (G) Comparison as in (C) between two replicates of the formaldehyde-crosslinked CASC3-EJC RIPiT-Seq samples [FLAG-CASC3:EIF4A3-xl, replicate B (x-axis) versus FLAG-CASC3:EIF4A3-xl, replicate A (y-axis)].
- (H) Comparison as in (C) between two replicates of the formaldehyde-crosslinked RNPS1-EJC RIPiT-Seq samples [FLAG-RNPS1:EIF4A3-xl, replicate B (x-axis) versus FLAG-RNPS1:EIF4A3-xl, replicate A (y-axis)].
- (I) Normalized read densities in alternate EJC footprint libraries in the genomic region indicated at the bottom. Each box plot comprises values from all eight RIPiT-Seq datasets listed in Table S2. Top: p-values (Wilcoxon rank sum test).
- (J) Meta-exon plots showing read depth in different RIPiT-Seq or RNA-Seq libraries (top left corner) in the 150 nucleotides (nt) from the exon 3' end.

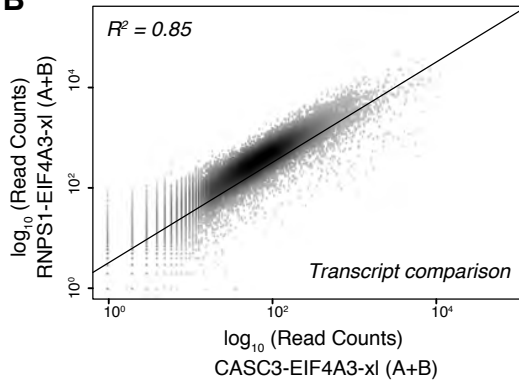
- (K) Distribution of exon mapping reads among the exonic regions indicated on top in the RIPiT-Seq libraries (bottom).
- (L) Cumulative distribution function plots showing frequency of reads in the indicated samples with the highest score for match to PWM for SRSF9 motif (inset, top right). Bottom left: sample identity. The SRSF9 motif shown in the inset is from (Paradis et al., 2007).
- (M) A negative binomial based assessment of significance of differences in SRSF9 motif PWM scores in (L) between reads from samples in the legend on the bottom left. Horizontal dotted red line: $p=0.05$; Horizontal solid red line: Bonferroni adjusted p -value.

Figure S4

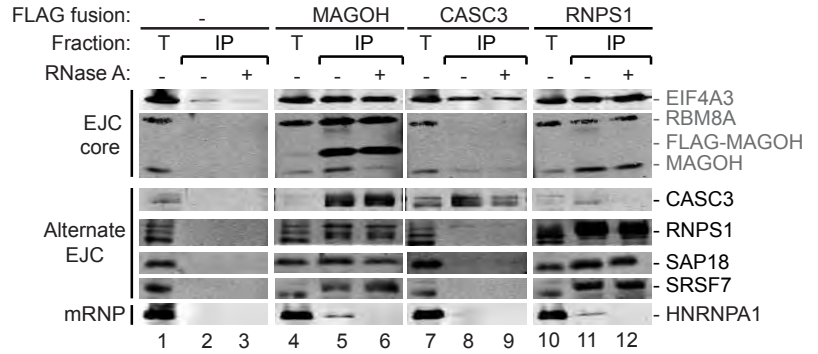
A



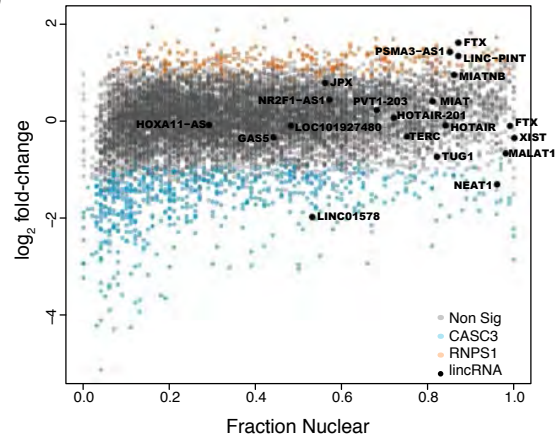
B



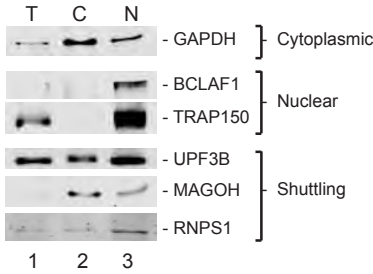
C



D



E



F

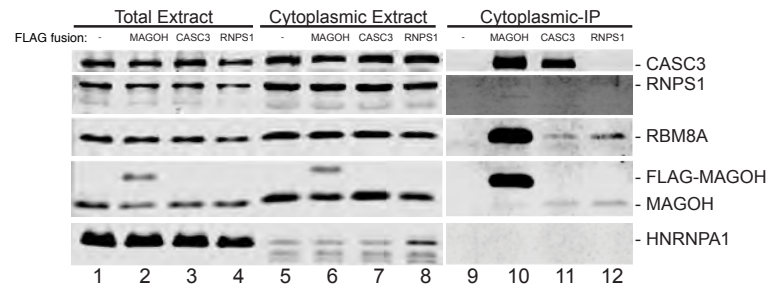


Figure S4. (related to Figure 4)

- (A) Comparison of read counts from both cross-linked replicates of CASC3-EJC (x-axis) versus RNPS1-EJC (y-axis). Each dot on the scatter plot represents each exon in the knownCanonical transcript annotation for UCSC known genes. A linear fit and coefficient of determination (R^2) are shown.
- (B) Comparison of read counts from both cross-linked replicates of CASC3-EJC (x-axis) versus RNPS1-EJC (y-axis). Each dot on the scatter plot represents knownCanonical transcript for UCSC known genes. A linear fit and coefficient of determination (R^2) are shown.
- (C) RNA dependent and independent interactions between EJC proteins. Western blots of proteins on the right in total extracts (T) or FLAG immunoprecipitates (IP) from HEK293 cells expressing FLAG-tagged proteins on the top. Inclusion of RNase A in extracts during IP is indicated on top of each lane.
- (D) Relative alternate EJC levels versus nuclear abundance of long non-coding RNAs (lncRNAs). Each dot on the scatter plot represents knownCanonical transcript with spliced lncRNAs labeled in black. CASC3 or RNPS1-enriched transcripts are colored as in the legend (bottom right). x-axis: -ve fold-change= CASC3-enrichment, +ve fold-change= RNPS1-enrichment.
- (E) Subcellular fractionation. Western blots for proteins on the right in total extracts (T), cytoplasmic (C), or nuclear (N) fractions of HEK293 cells.
- (F) Presence of alternate EJCs in cytoplasmic extracts. Western blots for proteins on the right in the fractions of HEK293 cells (top). FLAG-tagged proteins expressed in cells are indicated above each lane.

Figure S5

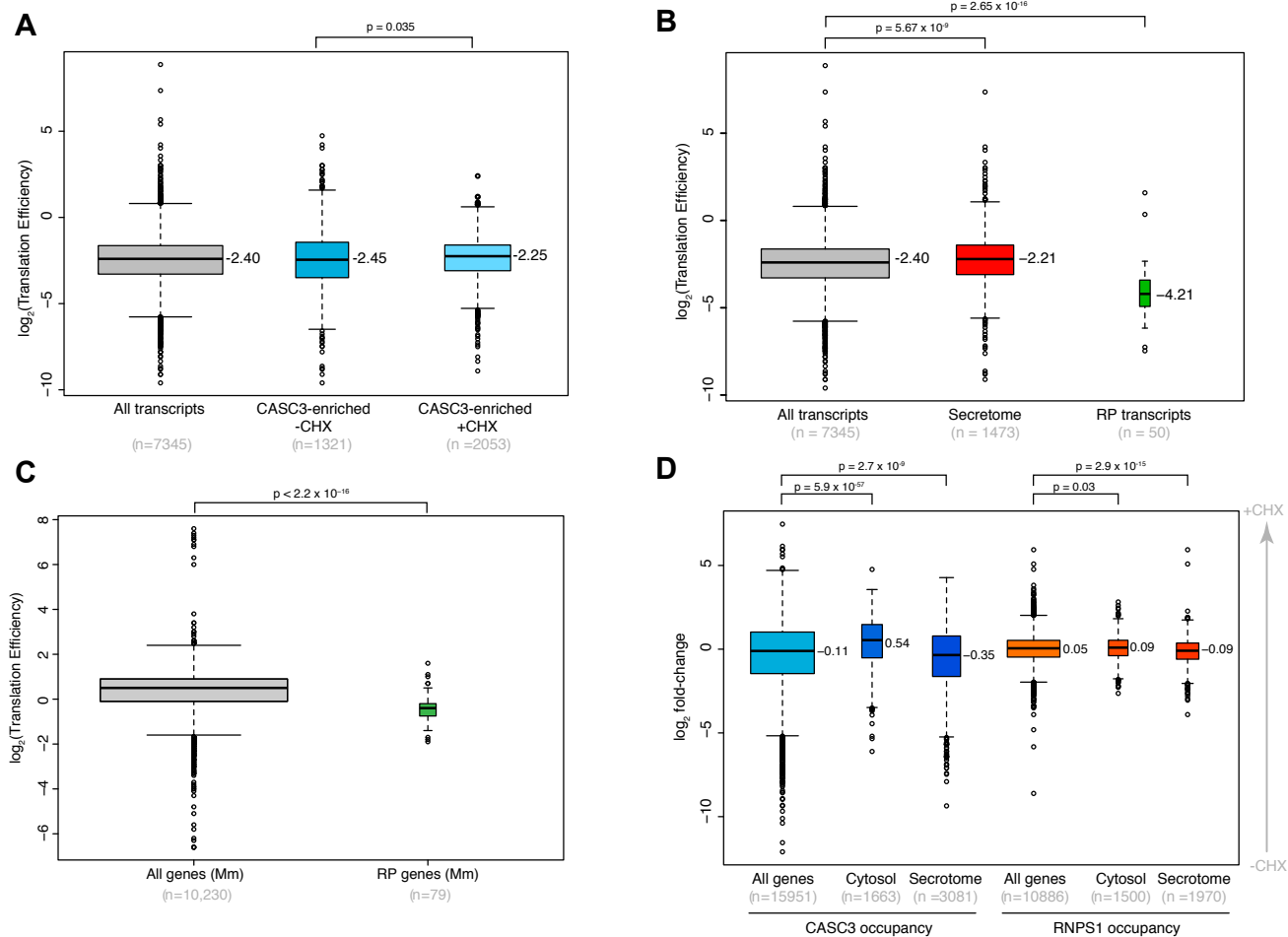
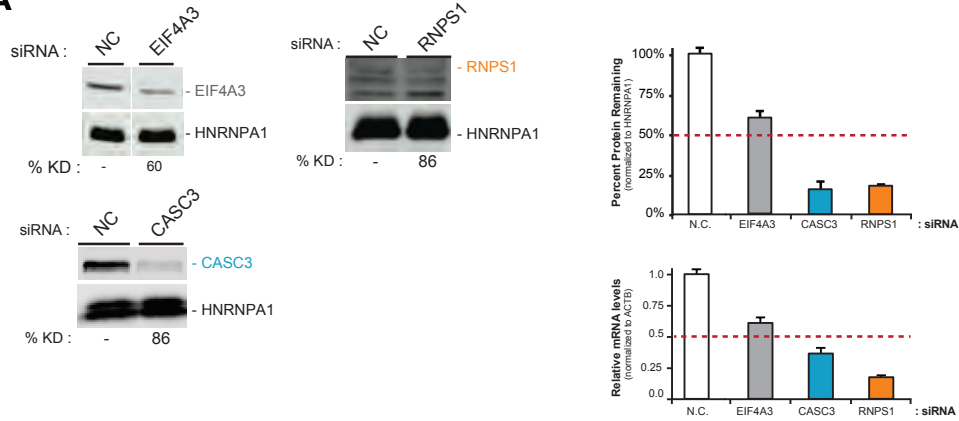


Figure S5. (related to Figure 5)

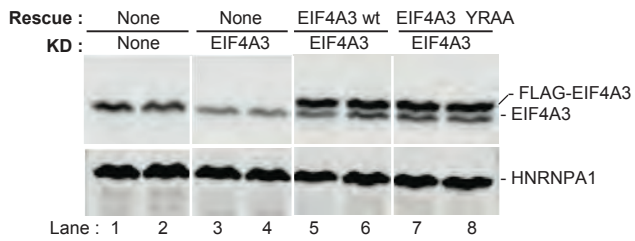
- (A) Box plots showing distribution of translation efficiency estimates (y-axis) of transcript groups on y-axis. The median values are given to the right of each box plot. Top: p-values (Wilcoxon rank sum test). Bottom: the number of transcripts in each group.
- (B) Comparison of translation efficiency (TE, y-axis) of secretome (red) and ribosomal protein (RP) transcripts (green) to all transcripts (grey). Number of genes in group are at the bottom. TE data from (Kiss et al., 2017).
- (C) Translation efficiency of RP genes in mouse embryonic stem cells. TE data from (Ingolia et al., 2011).
- (D) Box plots showing fold-change (y-axis) in alternate EJC occupancy (x-axis, at the bottom) for transcript groups shown at the bottom. x-axis: -ve fold-change= enrichment in -CHX condition, +ve fold-change= enrichment in +CHX condition. The median fold-change values are given to the right of each box plot. Top: p-values (Wilcoxon rank sum test). Bottom: the number of transcripts in each group.

Figure S6

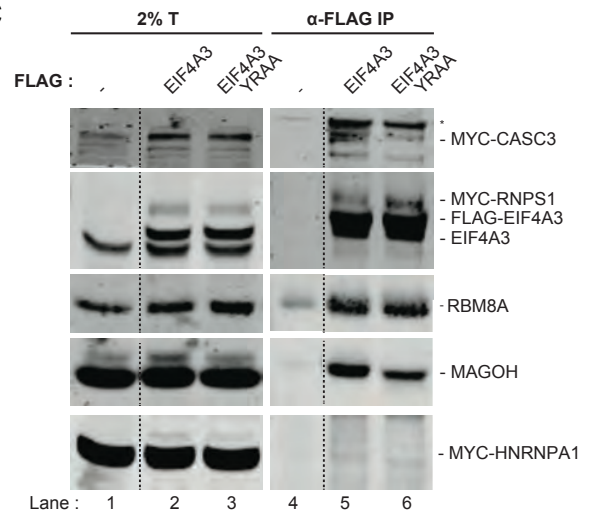
A



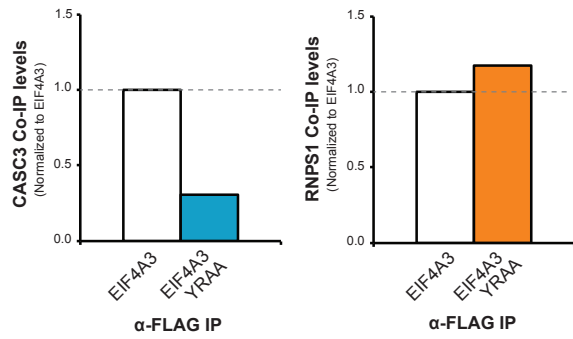
B



C



D



E

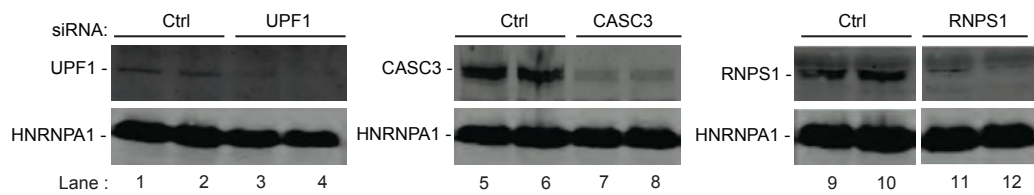


Figure S6 (related to Figure 6)

- (A) Knockdowns of EJC proteins (related to Figure 6A). Western blots of EJC core and alternate factor siRNA-mediated knockdowns (left). Right, top: Quantification of knockdown efficiency of EJC protein remaining relative to HNRNPA1 protein levels. Right, bottom: Knockdown efficiency as determined by qPCR of EJC factor mRNA levels relative to ACTB mRNA levels .
- (B) Rescue of EIF4A3-depleted cells. Western blots for proteins on the right from HEK293 cells depleted of EIF4A3 and expressing either wild-type EIF4A3 or a mutant EIF4A3 lacking CASC3 interaction as indicated on the top.
- (C) Interaction of EIF4A3-YRAA with CASC3. Western blots showing proteins on the right in total extract or FLAG IPs from HEK293 cells expressing FLAG-tagged proteins on the top along with MYC-CASC3, -RNPS1, and -HNRNPA1. The asterisk indicates cross-reacting band likely to be unreduced FLAG-IgG heavy chain.
- (D) Quantification of western blots in (C) showing relative MYC-CASC3 (left, blue) and MYC-RNPS1 (right, orange) co-IP with FLAG-EIF4A3 proteins on the bottom.
- (E) Knockdown of EJC/UPF1 proteins (Figure 6C). Western blots showing proteins indicated on the left from HeLa Tet-off cells treated with siRNAs indicated on the top. Two technical replicates of each knockdown are shown. HNRNPA1 panel shown in lanes 5-6 is shown again in lanes 9-10.

Figure S7

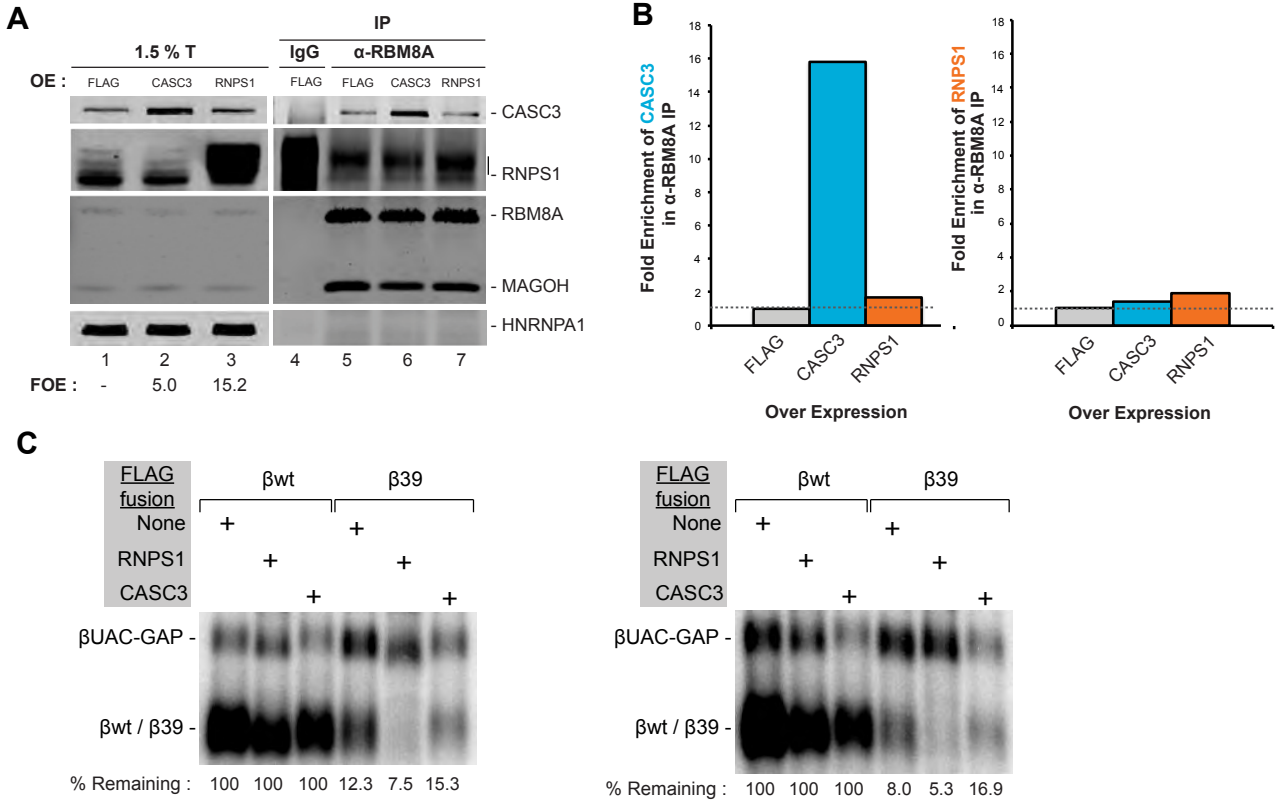


Figure S7 (related to Figure 7)

- (A) Effect of alternate EJC factor overexpression on EJC composition. Western blots for proteins on the right in total extract (lanes 1-3), control IgG IP (lane 4) or RBM8A IPs (lanes 5-7) from HEK293 cells overexpressing (OE) FLAG-fusion proteins at top. Fold overexpression (FOE) on bottom is relative to protein levels in lane 1 after normalizing to HNRNPA1 protein levels in particular lane.
- (B) Quantification of (A) for co-IP of CASC3 (left) or RNPS1 (right) upon RBM8A IP from cell lines overexpressing the proteins on the bottom. Fold enrichment was normalized by co-purifying MAGOH levels.
- (C) Effect of alternate EJC overexpression on β -globin NMD. Northern blots showing levels of wild-type β -globin RNA (β wt) and an NMD-targeted β -globin RNA (β 39) (as indicated on the top) along with co-transfected β UAC-GAP RNA from HeLa cells expressing alternate EJC factors (top left). % Remaining: β wt or β 39 levels in each sample were normalized to β UAC-GAP RNA. Numbers below each lane show normalized β 39 RNA remaining as % of normalized β wt RNA for the corresponding treatment (set to 100). Two independent replicates are shown.

Table S1. Summary of proteins identified by LC-MS/MS in the two replicates of FLAG-EJC and FLAG-only IPs.

#Alternate EJC_replicate1			
341 proteins at 99% minimum, 2 minimum peptides, 0.0% decoy FDR;; 9540 spectra at 95% minimum, 0.00% decoy FDR			
From proteins clusters, only member proteins with a non-zero value in at least one sample were retained			
Normalized spectral abundance factor (NSAF) values from Scaffold were used for quantitation; a psuedo count of 0.000001 was added to each NSAF value before determining enrichment in EJC IPs as compared to FLAG-only			
Proteins enriched >2-fold in any of the three EJC IPs over FLAG-only IP are shown			
	log2(NSAF)		
Accession Number	MAGOH	CASC3	RNPS1
SAP18_HUMAN	12.12344246	9.600730633	13.95255926
LC7L2_HUMAN	10.76661172	0	12.67785175
SRSF1_HUMAN	9.42840205	8.905056005	11.86905398
H4_HUMAN	12.27926234	12.49192823	11.75826486
SRSF6_HUMAN	11.27676417	0	11.69657638
PR40A_HUMAN	11.06379952	0	11.54245153
SCML1_HUMAN	0	0	11.46142829
PRP4B_HUMAN	11.4926043	0	11.23463783
RBM25_HUMAN	10.46954007	0	11.04753294
GPTC8_HUMAN	8.417008587	0	10.96275144
SNIP1_HUMAN	0	0	10.95325069
SRSF7_HUMAN	9.487699374	0	10.81338039
TRA2A_HUMAN	10.24210228	0	10.79100005
PPIG_HUMAN	8.82527683	0	10.73479428
DDX41_HUMAN	10.10105646	0	10.64988486
CWC22_HUMAN	10.55487659	0	10.10446771
SRS10_HUMAN	9.349303347	0	10.09037711
CRNL1_HUMAN	9.654385415	0	9.980853606
MGN_HUMAN	12.77585716	12.25168951	9.934059395
CATIN_HUMAN	9.81605565	0	9.879828273
CSK21_HUMAN	0	0	9.834897633
SRSF3_HUMAN	0	0	9.766512345
RBM8A_HUMAN	12.93774162	11.73564064	9.681238412
ANM1_HUMAN	8.887708033	0	9.628390857
SRSF5_HUMAN	9.295332732	0	9.621740545
CDK12_HUMAN	9.840982435	0	9.583195621
RPB1_HUMAN	10.1382718	0	9.572643389
RL6_HUMAN	10.21176665	12.0086037	9.539391485
PGAM5_HUMAN	9.208014828	0	9.534400161
CCNK_HUMAN	0	0	9.529430554
SRSF4_HUMAN	8.43629512	0	9.497971558
PLRG1_HUMAN	9.961290512	0	9.440786132
RBM22_HUMAN	9.668034004	0	9.410281737
ZC3HE_HUMAN	9.443979543	0	9.408329741

SRSF9_HUMAN	0	0	9.336752009
DHX8_HUMAN	10.1291542	0	9.331432034
H2AY_HUMAN	9.842915995	8.321612471	9.170726276
RU2A_HUMAN	0	0	9.130647779
H2A1A_HUMAN	0	0	9.091646948
RT29_HUMAN	0	0	9.073445375
ZCH18_HUMAN	9.807709112	0	9.036201092
SRSF8_HUMAN	0	0	8.985699652
SPT6H_HUMAN	7.634593268	0	8.957073013
NKTR_HUMAN	9.675904121	0	8.933572638
CD11A_HUMAN	0	0	8.834629058
CWC27_HUMAN	8.501837185	0	8.82791427
DGC14_HUMAN	0	0	8.815767536
AKP8L_HUMAN	8.050556113	0	8.790283326
RBBP6_HUMAN	6.588219912	0	8.77778133
FXR2_HUMAN	7.991748578	0	8.731352976
CSK22_HUMAN	0	0	8.674721924
HP1B3_HUMAN	9.271719795	7.75181182	8.599950025
LUC7L_HUMAN	0	0	8.590886411
SNUT2_HUMAN	0	0	8.569058109
FIP1_HUMAN	8.171226847	0	8.497053445
CMBL_HUMAN	0	12.08988078	8.190713617
SMU1_HUMAN	9.964095343	0	8.124793379
RS4X_HUMAN	0	9.818933622	8.088788239
NCBP1_HUMAN	0	0	8.0869854
PHRF1_HUMAN	9.017838416	0	8.025527183
SRRT_HUMAN	8.609437329	0	7.938462236
PAXB1_HUMAN	7.547434405	0	7.87276721
RBMX_HUMAN	0	0	7.519243094
GPTC1_HUMAN	7.525755693	0	7.269126679
REcq5_HUMAN	9.015526561	0	7.179610571
PPWD1_HUMAN	10.04644195	0	6.799993888
PININ_HUMAN	6.8673278	-6.910133013	6.25017964
IF4A3_HUMAN	6.771047915	6.220329511	6.19106795
DDB1_HUMAN	0	8.704906538	5.99047842
SON_HUMAN	6.126682474	-5.179948888	5.676165346
TCOF_HUMAN	0	7.326069892	5.61303063
SFR19_HUMAN	5.367405791	-6.048388784	4.575401278
SRRM1_HUMAN	4.360907368	0.470829819	4.257178256
RNPS1_HUMAN	3.31613842	-0.526593813	4.227919599
ACINU_HUMAN	4.051882067	-1.108281217	4.080682378
LC7L3_HUMAN	3.797146519	-7.636334602	4.053576036
RBM39_HUMAN	3.799733114	-8.33860269	3.82174148
TRA2B_HUMAN	3.801634108	-9.216479117	3.594192925
PUF60_HUMAN	1.989468646	1.466254652	3.314884359
RPB2_HUMAN	3.56347561	-6.206428335	3.305719523
PCBP1_HUMAN	1.992068594	2.052717845	3.192553494
SRRM2_HUMAN	3.974038446	-2.821225465	3.167279714
SNW1_HUMAN	1.989809969	0.46980974	3.052499512

PRP17_HUMAN	2.573419515	-7.216260837	2.899953146
RL3_HUMAN	2.5786637	1.470114407	2.735523603
TR150_HUMAN	2.749709192	-9.486633935	2.409244244
BCLF1_HUMAN	2.802239395	-9.54041868	2.26048122
SYF1_HUMAN	2.453011539	-1.520974484	2.259183547
U2AF2_HUMAN	0.994555861	-8.496174702	2.057358601
GNL3_HUMAN	0.991971421	0.46977667	2.053387389
HNRPF_HUMAN	2.575736378	2.466527005	1.733568579
AQR_HUMAN	1.408956925	-8.436878077	1.674127144
XRCC6_HUMAN	0.581108117	-0.941562133	1.322646441
PRP8_HUMAN	1.132917086	-3.823514146	1.143372415
CLK3_HUMAN	0.993848117	-8.071944968	1.057569892
OAT_HUMAN	-9.929302799	2.734055165	1.000769209
CDC5L_HUMAN	2.073375358	-9.907942177	0.960108676
H2A1J_HUMAN	0.58130639	1.056951881	0.738216988
ODB2_HUMAN	0.994496198	2.638771496	0.736795312
TBA1A_HUMAN	-7.574555686	2.466145001	0.735420807
NOP56_HUMAN	0.991616276	0.469501869	0.734475527
HS71L_HUMAN	0.991118205	0.469252722	0.734107857
SSRP1_HUMAN	0.99505304	-1.522078189	0.544862646
PPM1B_HUMAN	0.20003204	1.577484201	0.308705987
U5S1_HUMAN	1.298784908	-2.846251758	0.290901674
SP16H_HUMAN	1.315840207	-1.519385898	0.060224306
CASC3_HUMAN	11.73089465	13.48645796	0
WIBG_HUMAN	11.70852352	10.18512321	0
CCDC9_HUMAN	9.914400082	0	0
RL5_HUMAN	9.168697186	10.22809716	0
REN3B_HUMAN	8.468705491	10.74852832	0
BOLA2_HUMAN	0	12.01531051	0
RL13_HUMAN	0	10.13647852	0
RO52_HUMAN	0	9.551362204	0
P53_HUMAN	0	9.24026662	0
PRDX2_HUMAN	0	9.229299509	0
GSHR_HUMAN	0	8.831528936	0
C1TM_HUMAN	0	8.511475946	0
TBB2A_HUMAN	0	8.063988217	0
LAP2A_HUMAN	0	7.425845306	0
EF1A1_HUMAN (+1)	-0.22569663	1.249191701	-0.068927127
TBB5_HUMAN	-0.00348044	0.986567489	-0.161984954
IRS4_HUMAN	0.986035447	2.776196272	-0.257407108
DJC10_HUMAN	-6.766065051	1.463811228	-0.258872981
RS8_HUMAN	2.578589362	1.470068567	-0.26084481
EFTU_HUMAN	0.410946763	1.692939326	-0.261061789
STK38_HUMAN	-0.003433705	1.056732389	-0.261408701
REST_HUMAN	-1.3198622	1.848156873	-0.581625339
CK084_HUMAN	-11.39580187	1.346444398	-0.676241922
RL4_HUMAN	1.731826571	2.344806224	-0.844616109
TBA4A_HUMAN	-0.003471556	1.055272517	-1.256318815

ILF2_HUMAN	-8.779916297	1.055549917	-1.256981736
SERA_HUMAN	-0.225705018	0.986138055	-1.481694665
CLAP2_HUMAN	-0.58481771	2.051714144	-1.827854863
HNRPL_HUMAN	-8.770135276	1.470179053	-1.837979591
E2F7_HUMAN	-9.140190703	1.055919581	-1.839883907
SERPH_HUMAN	-7.683626283	1.467796235	-7.683626283
HDAC6_HUMAN	-0.584962501	1.689961089	-7.72900887
AIFM1_HUMAN	-8.129386063	1.054571811	-8.129386063

#Alternate EJC_replicate2			
175 proteins at 99% minimum, 2 minimum peptides, 0.0% decoy FDR;; 7282 spectra at 95% minimum, 0.00% decoy FDR			
From proteins clusters, only member proteins with a non-zero value in at least one sample were retained			
Normalized spectral abundance factor (NSAF) values from Scaffold were used for quantitation; a psuedo count of 0.000001 was added to each NSAF value before determining enrichment in EJC IPs as compared to FLAG-only			
Proteins enriched >2-fold in any of the three EJC IPs over FLAG-only IP are shown			
	log2(NSAF)		
Accession Number	Magoh	MLN51	RNPS1
IF4A3_HUMAN	13.7638348	11.03967305	13.42245903
RNPS1_HUMAN	12.09199728	0	13.31783654
MGN_HUMAN	14.55895875	10.9479291	12.93590168
SMD1_HUMAN	11.36260139	0	12.86834029
PININ_HUMAN	13.14623453	0	12.80982841
H2A1D_HUMAN (+6)	12.04217235	0	12.74081375
ACINU_HUMAN	12.39159267	0	12.71647653
H4_HUMAN	0	0	12.5912652
RU2A_HUMAN	10.8482317	12.3128546	12.48507456
SRSF7_HUMAN	11.68439798	0	12.23101112
SRSF1_HUMAN	11.30320995	0	12.08921873
SAP18_HUMAN	11.32198445	0	12.02049387
LC7L3_HUMAN	11.50248377	0	12.00842862
RBM39_HUMAN	11.5997734	0	11.9935753
SF3B1_HUMAN	11.7159191	11.37378957	11.79709406
SMD3_HUMAN	0	0	11.78610623
TRA2B_HUMAN	10.6727789	0	11.69300772
U5S1_HUMAN	11.46183752	0	11.67511904
RBM25_HUMAN	11.0617087	0	11.52214012
PRP19_HUMAN	12.03479896	0	11.43827206
RUXE_HUMAN	0	0	11.4325941
SRRM1_HUMAN	11.72250872	0	11.38392025
TR150_HUMAN	11.78418496	0	11.26631806
SRRM2_HUMAN	11.4604559	0	11.23038076
H13_HUMAN	0	12.51929225	11.16835873
SRSF9_HUMAN	0	0	11.16835873

LC7L2_HUMAN	10.64304445	0	11.1489214
PR40A_HUMAN	10.74760559	0	11.14134082
RSMB_HUMAN (+1)	9.352175878	11.55252501	11.04937211
RU2B_HUMAN	0	11.32378662	10.94989965
PRP4B_HUMAN	9.453003062	0	10.93472289
SRSF3_HUMAN	10.48522554	0	10.92072502
U520_HUMAN	9.841595796	0	10.89565101
BCLF1_HUMAN	11.90358063	0	10.86581058
SRSF6_HUMAN	9.832177982	0	10.70017959
SMD2_HUMAN	0	0	10.65883628
SNR40_HUMAN	10.7779128	0	10.64664871
SF3B6_HUMAN	0	0	10.57572832
H2B1C_HUMAN (+8)	0	10.16100588	10.56424478
SF3A2_HUMAN	11.20683123	10.28019079	10.55803798
U2AF2_HUMAN	9.688757349	0	10.52424786
PPIG_HUMAN	9.700179593	0	10.39820926
DDX41_HUMAN	10.78422586	0	10.37634248
SNW1_HUMAN	10.89193556	0	10.35005518
FIP1_HUMAN	0	0	10.32732808
CDC5L_HUMAN	11.13359178	0	10.30924896
PCBP1_HUMAN	9.782768932	0	10.28840471
SRS10_HUMAN	10.54631572	0	10.24531501
RS4X_HUMAN	10.21916852	0	10.23983717
SCML1_HUMAN	0	0	10.17990909
RBMX_HUMAN	10.45419646	0	10.15317199
PRP8_HUMAN	8.771390425	0	10.12528431
CH60_HUMAN	11.00204143	0	10.11647393
RBM22_HUMAN	10.54361188	0	10.05012073
XRCC6_HUMAN	0	0	9.876777836
H33_HUMAN	0	0	9.86968637
TRA2A_HUMAN	0	0	9.817655232
RIOK1_HUMAN	10.27821712	10.79547151	9.807483728
BUD31_HUMAN	0	0	9.787314917
CCNK_HUMAN	9.66370041	0	9.777353958
SON_HUMAN	9.968090752	0	9.757306662
GRP75_HUMAN	10.5510353	0	9.71998768
RS18_HUMAN	0	0	9.709411269
AQR_HUMAN	9.307861087	0	9.669062209
RL7_HUMAN	0	0	9.588246152
RL7A_HUMAN	0	0	9.487297414
XRCC5_HUMAN	0	0	9.441989675
ISY1_HUMAN	9.688757349	0	9.387909618
PGAM5_HUMAN	9.08459582	0	9.367829698
RS2_HUMAN	9.064796646	10.52816105	9.348042047
CSK21_HUMAN	0	0	9.3468018
SNIP1_HUMAN	8.631140669	0	9.328495421
SMU1_HUMAN	10.42500604	0	9.277054876

SR140_HUMAN	9.421854445	10.59039992	9.272839701
PR38A_HUMAN	0	0	9.257529276
RLA0_HUMAN	9.535430915	8.831845581	9.234625857
GPTC8_HUMAN	0	0	9.21273955
SFR19_HUMAN	8.226074963	0	9.185494924
SNUT1_HUMAN	7.620366471	0	9.121714814
PAXB1_HUMAN	9.003855181	0	9.117435318
H2A1A_HUMAN (+2)	0	0	8.925168681
RL3_HUMAN	0	0	8.888986721
HNRH1_HUMAN	9.034001065	0	8.733388238
TBA1B_HUMAN	9.027601948	0	8.727001465
PPIE_HUMAN	0	0	8.725400344
HNRPC_HUMAN	10.00084508	10.4655664	8.701687664
GRP78_HUMAN	9.490690457	0	8.6061831
PLRG1_HUMAN	8.255972742	0	8.538848521
RED_HUMAN	8.72369507	0	8.423241996
CDK12_HUMAN	7.722602637	0	8.418738108
PRP17_HUMAN	10.08081753	0	8.3675458
DDX21_HUMAN	8.647602329	0	8.347178416
RBBP6_HUMAN	7.04537744	0	8.322694323
SPF45_HUMAN	10.61028666	10.07588021	8.312701473
NKAP_HUMAN	0	0	8.263363107
RL4_HUMAN	9.842271763	0	8.22360218
SYF1_HUMAN	8.842161743	0	8.220668531
SRRT_HUMAN	8.072427412	0	8.185767456
MFAP1_HUMAN	0	0	8.182493675
OAT_HUMAN	0	0	8.182493675
CWC22_HUMAN	8.434503133	0	8.13422094
EF1A1_HUMAN (+1)	8.409348503	0	8.109099329
SRS11_HUMAN	0	0	8.04220656
HNRPM_HUMAN	9.33230514	0	8.034358798
DHX8_HUMAN	0	0	8.03039126
ZC3HE_HUMAN	9.734997453	0	8.022589749
SPTN1_HUMAN	8.574139362	6.877866923	8.011674533
TAB1_HUMAN	8.867618521	9.162265434	7.984019633
MATR3_HUMAN	0	0	7.820753373
CRNL1_HUMAN	8.119096751	0	7.819029455
CHERP_HUMAN	8.008204497	0	7.708256223
CDK13_HUMAN	0	0	7.401903472
MYH9_HUMAN	9.229515825	9.372473325	7.34978987
TBB4B_HUMAN	9.046878442	8.343807528	7.168020189
ZCH18_HUMAN	0	0	7.070067262
NKTR_HUMAN	0	0	7.037821465
IPO8_HUMAN	8.564416278	8.124017889	6.949184722
CAMP3_HUMAN	0	0	6.683134985
MAP1B_HUMAN	0	0	6.29000041
SPTB2_HUMAN	6.649256178	0	5.775182264

FLNA_HUMAN	7.218393711	0	5.615210284
IF4B_HUMAN	2.319331128	3.873106719	1.625925187
RBM8A_HUMAN	11.39943816	0	0
CASC3_HUMAN	11.19241612	12.26488238	0
CCDC9_HUMAN	10.20554891	0	0
COR1C_HUMAN	9.691795853	10.24946904	0
REN3B_HUMAN	9.664678382	0	0
PYM1_HUMAN	9.586314394	0	0
HNRPK_HUMAN	8.989791843	0	0
HNRPR_HUMAN	8.953701754	0	0
SRSF4_HUMAN	8.896483781	0	0
SLU7_HUMAN	8.65065687	0	0
FL2D_HUMAN	8.631140669	0	0
HNRPF_HUMAN	8.563692024	0	0
OTUD4_HUMAN	7.727103604	0	0
LIMA1_HUMAN	7.695854658	8.572851782	0
TBA1C_HUMAN	7.454504938	0	0
K2C8_HUMAN	7.349878311	0	0
TMOD3_HUMAN	0	11.26315181	0
PRDX1_HUMAN	0	11.0860035	0

Table S2. Summary of all described RIPiT-Seq and RNA-Seq libraries.

*All numbers represent unique counts
 **Tables A-D show counts in sequential order of processing

Table A. Multi-mapping and PCR duplicate read removal

Library	TopHat Input Total	Mapped	(%)	Multi-Mapped	(%)	Input Reads	Multi-Mappers	(%)	PCR Duplicates	(%)
MAGOH-EIF4A3	12289132	11788001	95.92	919103	7.8	11788001	919103	7.8	38395	0.33
CASC3-EIF4A3	7918724	7552965	95.38	501748	6.64	7552965	501748	6.64	14235	0.19
RNPS1-EIF4A3	9353236	8964991	95.85	921854	10.28	8964991	921854	10.28	16528	0.18
MAGOH-CASC3	6792045	6423758	94.58	408153	6.35	6423758	408153	6.35	31314	0.49
MAGOH-RNPS1	11996168	11169040	93.11	617910	5.53	11169040	617910	5.53	35527	0.32
CASC3-EIF4A3-XL-A	5718072	5309270	92.85	370143	6.97	5309270	370143	6.97	10068	0.19
CASC3-EIF4A3-XL-B	21898851	20055735	91.58	3554071	17.72	20055735	3554071	17.72	2013494	10.04
RNPS1-EIF4A3-XL-A	8370005	7838852	93.65	651639	8.31	7838852	651639	8.31	23133	0.3
RNPS1-EIF4A3-XL-B	24859586	23434622	94.27	4666719	19.91	23434622	4666719	19.91	715018	3.05
CASC3-EIF4A3-XL-A (+CHX)	15795694	15084794	95.5	684318	4.54	15084794	684318	4.54	182916	1.21
CASC3-EIF4A3-XL-B (+CHX)	13937900	13413713	96.24	523380	3.9	13413713	523380	3.9	75455	0.56
RNPS1-EIF4A3-XL-A (+CHX)	27687914	26580410	96	2258708	8.5	26580410	2258708	8.5	187891	0.71
RNPS1-EIF4A3-XL-B (+CHX)	2532100	2274851	89.84	95329	4.19	2274851	95329	4.19	26077	1.15
RNA-Seq-A	18740947	12180518	64.99	4873419	40.01	12180518	4873419	40.01	58947	0.48
RNA-Seq-B	19476485	12592943	64.66	4811993	38.21	12592943	4811993	38.21	46021	0.37

Table B. Removal of miscellaneous RNAs

Library	Mitochondrial	(%)	miRNA	(%)	(%)	rRNA (+ChrUn)	(%)	scaRNA	(%)	snoRNA	(%)	snRNA	(%)	tRNA	(%)	Final Count
MAGOH-EIF4A3	144700	1.23	1384	0.01	0	3524726	29.9	396	0	20182	0.17	677876	5.75	2223	0.02	6459016
CASC3-EIF4A3	124075	1.64	787	0.01	0	4946036	65.48	102	0	4582	0.06	462939	6.13	3095	0.04	1495366
RNPS1-EIF4A3	108423	1.21	879	0.01	0	3215430	35.87	193	0	7039	0.08	1275182	14.22	3955	0.04	3415508
MAGOH-CASC3	35630	0.55	936	0.01	0	3663566	57.03	105	0	3038	0.05	163479	2.54	4305	0.07	2113232
MAGOH-RNPS1	60106	0.54	1511	0.01	0	5766613	51.63	133	0	4938	0.04	385709	3.45	4516	0.04	4292077
CASC3-EIF4A3-XL-A	22902	0.43	1264	0.02	0	3382695	63.71	322	0.01	7479	0.14	140262	2.64	3892	0.07	1370243
CASC3-EIF4A3-XL-B	98373	0.49	3261	0.02	0	11708237	58.38	1866	0.01	6384	0.03	1297149	6.47	10183	0.05	1362717
RNPS1-EIF4A3-XL-A	28638	0.37	1455	0.02	0	3253080	41.5	896	0.01	16125	0.21	506409	6.46	4484	0.06	3352993
RNPS1-EIF4A3-XL-B	50751	0.22	6254	0.03	0	9460234	40.37	3923	0.02	13060	0.06	2295813	9.8	8177	0.03	6214673
CASC3-EIF4A3-XL-A (+CHX)	47903	0.32	14652	0.1	0	4289703	28.44	334	0	7472	0.05	76118	0.5	8924	0.06	9772454
CASC3-EIF4A3-XL-B (+CHX)	60192	0.45	6725	0.05	0	4702167	35.05	243	0	4686	0.03	71546	0.53	6357	0.05	7962962
RNPS1-EIF4A3-XL-A (+CHX)	132946	0.5	2653	0.01	0	12002630	45.16	1679	0.01	36309	0.14	1267031	4.77	21014	0.08	10669549
RNPS1-EIF4A3-XL-B (+CHX)	3478	0.15	110	0	0	1526002	67.08	49	0	235	0.01	9165	0.4	93	0	614313
RNA-Seq-A	507860	4.17	11319	0.09	0	693781	5.7	5463	0.04	183690	1.51	481999	3.96	1883466	15.46	3480574
RNA-Seq-B	535924	4.26	13299	0.11	0	506876	4.03	6870	0.05	298611	2.37	673413	5.35	1945855	15.45	3754081

Table C. Genomic read distribution (51% overlap)

Library	Exonic	(%)	RPKM	Intronic	(%)	RPKM	Intergenic	(%)	1 Exon Genes	RPKM	2+ Exon Genes	RPKM
MAGOH-EIF4A3	4384496.00	67.88	7.40	1797361.00	27.83	0.19	277159.00	4.29	30122.00	1.70	4473662.00	7.78
CASC3-EIF4A3	906277.00	60.61	6.61	504613.00	33.75	0.23	84476.00	5.65	11554.00	2.82	924113.00	6.94
RNPS1-EIF4A3	2162371.00	63.31	6.90	1098461.00	32.16	0.22	154676.00	4.53	23011.00	2.46	2209957.00	7.27
MAGOH-CASC3	1476411.00	69.87	7.61	531464.00	25.15	0.17	105357.00	4.99	15495.00	2.68	1505597.00	8.00
MAGOH-RNPS1	3046675.00	70.98	7.74	1026440.00	23.91	0.16	218962.00	5.10	30176.00	2.57	3105684.00	8.13
CASC3-EIF4A3-XL-A	914747.00	66.76	7.28	379830.00	27.72	0.19	75666.00	5.52	7480.00	1.99	936445.00	7.68
CASC3-EIF4A3-XL-B	1193285.00	87.57	9.54	692445.00	50.81	0.34	523013.00	38.38	16125.00	4.32	1231702.00	10.15
RNPS1-EIF4A3-XL-A	2274827.00	67.84	7.39	908998.00	27.11	0.18	169168.00	5.05	15559.00	1.70	2336427.00	7.83
RNPS1-EIF4A3-XL-B	7357943.00	118.40	12.90	3281206.00	52.80	0.36	4424476.00	71.19	53784.00	3.16	7573547.00	13.69
CASC3-EIF4A3-XL-A (+CHX)	7860415.00	80.43	8.77	1741791.00	17.82	0.12	170248.00	1.74	47235.00	1.77	8010464.00	9.21
CASC3-EIF4A3-XL-B (+CHX)	6528217.00	81.98	8.94	1331364.00	16.72	0.11	103381.00	1.30	26773.00	1.23	6674856.00	9.42
RNPS1-EIF4A3-XL-A (+CHX)	7057878.00	66.15	7.21	3096590.00	29.02	0.20	515081.00	4.83	46214.00	1.58	7205508.00	7.59
RNPS1-EIF4A3-XL-B (+CHX)	454507.00	73.99	8.06	117397.00	19.11	0.13	42409.00	6.90	4588.00	2.73	463153.00	8.47
RNA-Seq-A	1059522.00	30.44	3.32	1761478.00	50.61	0.34	659574.00	18.95	81172.00	8.52	1064409.00	3.44
RNA-Seq-B	1080657.00	28.79	3.14	1785669.00	47.57	0.32	887755.00	23.65	110593.00	10.76	1072926.00	3.21

Table D. Canonical/Non-canonical read classification

Library	Canonical	(%ofExonic)	Non-Canonical	(%ofExonic)	Uncounted	(%ofExonic)
MAGOH-EIF4A3	1546096.00	35.26	2722620.00	62.10	115780.00	2.64
CASC3-EIF4A3	289135.00	31.90	579485.00	63.94	37657.00	4.16
RNPS1-EIF4A3	811486.00	37.53	1267130.00	58.60	83755.00	3.87
MAGOH-CASC3	476638.00	32.28	951547.00	64.45	48226.00	3.27
MAGOH-RNPS1	898705.00	29.50	2006039.00	65.84	141931.00	4.66
CASC3-EIF4A3-XL-A	326669.00	35.71	530307.00	57.97	57771.00	6.32
CASC3-EIF4A3-XL-B	587174.00	49.21	543975.00	45.59	62136.00	5.21
RNPS1-EIF4A3-XL-A	723741.00	31.82	1407464.00	61.87	143622.00	6.31
RNPS1-EIF4A3-XL-B	2555021.00	34.72	4178245.00	56.79	624677.00	8.49
CASC3-EIF4A3-XL-A (+CHX)	2386087.00	30.36	4692151.00	59.69	782177.00	9.95
CASC3-EIF4A3-XL-B (+CHX)	3145982.00	48.19	2672452.00	40.94	709783.00	10.87
RNPS1-EIF4A3-XL-A (+CHX)	1593969.00	22.58	4853509.00	68.77	610400.00	8.65
RNPS1-EIF4A3-XL-B (+CHX)	46447.00	10.22	358889.00	78.96	49171.00	10.82

Table S3. List of reagents (siRNA sequences, qRT-PCR primers, antibodies, plasmids)

siRNAs

Gene	siRNA sequence	Reference
<i>AllStars Negative Control</i>	<i>Qiagen proprietary sequence</i>	
<i>EIF4A3_187</i>	CGA GCA AUC AAG CAG AUC AUU	This Study
<i>CASC3_534</i>	CCA GCA UAC AUA CCU CGG AUU	This Study
<i>RNPS1_2</i>	GCA UCC AGC CGC UCA GGA AUU	This Study

qRT-PCR primers

Gene	Primer (Forward)	Primer (Reverse)	Reference
<i>GADD45A</i>	GAGCTCCTGCTCTTGAGAC	GCAGGATCCTTCCATTGAGA	This Study
<i>UPP1</i>	CCAGCCTTGTTTGGAGATGT	ACATGGCATAGCGGTCAGTT	This Study
<i>ARC</i>	CTGAGATGCTGGAGCACGTA	GCCTTGATGGACTTCTTCCA	This Study
<i>DNAJB2</i>	TGGCATCCTACTACGAGATCC	GTTTTGTCTGGGTGCCACT	This Study
<i>eIF4A2</i>	TGTGGAGACGGTGACAGATTC	TTCCTGCTTTACCCACCAGTAC	This Study
<i>TMEM33</i>	AGGGTCAAGTCGTGTTCTGATC	ACCAACTGCTGCTATCGACTC	This Study
<i>SF3B1</i>	CACGGCAATGTGGCTTTCTC	ACTCACCAAGAAGAGGCAGAAC	This Study
<i>CAPN7</i>	AATTTCCCAGAGCGTCTTG	TTCGTGCCTTTGTCTCCATC	This Study
<i>TPT1</i>	CAACGGGAAGGCGAGCTCTC	GGAAGGAGCGGCAAAGTTTAC	This Study
<i>C1orf37</i>	TCATCAGCCATGGTCAGTAGG	TGCAGGTGATGGTTTCATGAC	This Study
<i>SRSF2</i>	TTGCTGCTCGAATCTCCAAG	ACTTCTGCTGCCATCACAAC	Lareau et al., 2007
<i>SRSF4</i>	CCTCTTAAGAAAATGCTGCGGTCTC	ATCAGCCAAATCAGTTAAAATCTGC	Lareau et al., 2007
<i>SRSF6</i>	GGATCTGAAGAACGGTCTGTTATGT	TCACTCGTCTTTTGGTTCCCATTAG	Lareau et al., 2007
<i>RPL3</i>	TGGTGGAAAAGTCTCTTAG	TCAGGAGCAGAGCAGAGTTG	This Study
<i>RPL12</i>	CTGGGCCTTAGCTTCTTCAC	AAGTGGCACCGACTTCACCT	This Study
<i>ACTB</i>	CGCGAGAAGATGACCCAGAT	TCACCGGAGTCCATCACGAT	This Study

Antibodies

Protein	Source	Catalog#
CASC3	Bethyl Laboratories	A302-472
RNPS1	Sigma Aldrich	HPA044014
RNPS1	Akila Mayeda	
EIF4A3	Bethyl Laboratories	A302-980A
HNRNPA1	Santa Cruz Biotechnology	SC-32301
ACIN1	Bethyl Laboratories	A300-999A
SAP18	Santa Cruz Biotechnology	SC-25377
RBM8A	Sigma Aldrich	Y1253 (4C4)
MAGOH	Santa Cruz Biotechnology	SC-271365
SRSF1	Santa Cruz Biotechnology	SC-33652
FLAG	Sigma Aldrich	F1804

Reagents

Reagent	Source	Catalog#
Protein A Dynabeads	Life Technologies	10002D
Protein G Dynabeads	Life Technologies	10003D
FLAG-Agarose Beads	Sigma Aldrich	A2220
FLAG peptide	Sigma Aldrich	F3290
MWCO 7,000 Da Dialysis Column	Pierce	88242
4X Lammelli SDS load buffer	Bio-Rad	161-0737
4%–15% Mini-PROTEAN TGX	Bio-Rad	4561086
Trypsin Gold	Promega	V5280
ProteaseMAX™ Surfactant	Promega	V2071
TransIT-X2	Mirus	MIR 6003
RNAiMAX	Thermo Fisher	13778030
JetPrime	PolyPlus	114-01
oligo-(dT)15 Primer	Promega	C1101
Superscript III	Invitrogen	18080044
Ribonuclease H	Promega	M4281
2X SYBR Green Master Mix	Applied Biosystems	4309155
RNase I	Promega	M4261
Ribo-Zero rRNA Removal Kit (H/M/R)	Illumina	MRZH116

Plasmids

Plasmid	Reference
pc β wt β	Lykke-Andersen, 2000
pc β 39 β	Lykke-Andersen, 2000
pcTET2- β wt β	Singh et al., 2007
pcTET2- β 39 β	Singh et al., 2007
pc β wtGAP3UAC	Lykke-Andersen, 2000
pcDNA3	Singh et al., 2012
pcDNA3 YFP	This study
pcDNA3 FLAG	Singh et al., 2012
pcDNA3 FLAG-EIF4AIII	Singh et al., 2012
pcDNA3 FLAG-EIF4AIII YRAA	This study
pcDNA3 FLAG-MAGOH	Singh et al., 2012
pcDNA3 FLAG-RNPS1	This study
pcDNA3 FLAG-CASC3	This study
pcDNA3 FLAG-HNRNPA1	This study
pcDNA5 FLAG-MAGOH	Singh et al., 2012
pcDNA5 FLAG-RNPS1	This study
pcDNA5 FLAG-CASC3	This study

EXPERIMENTAL PROCEDURES

Plasmids, Cell lines and cell culture

Plasmids expressing EJC factors and hnRNPA1 were generated by cloning their cDNAs into derivatives of pcDNA3.1 (for transient expression) or pcDNA5-FLAG-FRT/TO (for stable expression) as described previously (Singh et al., 2012). Plasmids expressing β -globin reporters have been described elsewhere (Lykke-Andersen, 2000; Singh, 2007). Human cell lines (HEK293 Flp-In TRex, HeLa CCL2, HeLa Tet-off) were cultured in Dulbecco's modified eagle medium (DMEM) supplemented with 10 % fetal bovine serum (FBS) and 1 % penicillin-streptomycin. Stable cell lines expressing tetracycline-inducible FLAG-tagged proteins were created using HEK293 Flp-In TRex cells as described previously (Singh et al., 2012).

Endogenous Immunoprecipitations

HEK293, HeLa and P19 cells were lysed and sonicated in hypotonic lysis buffer (HLB) [20 mM Tris-HCl pH 7.5, 15 mM NaCl, 10 mM EDTA, 0.5 % NP-40, 0.1 % Triton X-100, 1 x Sigma protease inhibitor cocktail, 1 mM PMSF]. Lysates were sonicated, increased to 150 mM NaCl and treated with RNase A for five minutes. Complexes were then captured on Protein A/G Dynabeads (Life Technologies) conjugated to IgG, α -EIF4A3, α -CASC3 or α -RNPS1 antibodies for 2 hr nutating at 4 °C. Complexes were washed in isotonic wash buffer (IsoWB) [20 mM Tris-HCl pH 7.5, 150 mM NaCl, 0.1 % NP-40] and eluted in clear sample buffer [100 mM Tris-HCl pH 6.8, 4 % SDS, 10 mM EDTA, 100 mM DTT]. Cortical neurons were isolated from FBV wild-type male mice in HBSS buffer. Once isolated, lysate preparation was carried out as stated above.

FLAG Immunoprecipitations

Stable HEK293 cells expressing FLAG-tagged EJC protein were lysed in HLB. Lysates were sonicated, increased to 150 mM NaCl and treated with RNase A. Complexes were then captured on FLAG-beads, washed with IsoWB and FLAG-peptide eluted. IPs were carried out as noted above.

Mass Spectrometry

FLAG Immunoprecipitation

Stably expressed FLAG-MAGOH, FLAG-CASC3, FLAG-RNPS1, or FLAG-peptide were IPed and RNase A digested at 4 °C for 2 hr in lysis buffer supplemented with 1 µg/ml FLAG peptide to improve IP specificity. The FLAG affinity elution was completely dried by vacuum evaporation, re-suspended in 100 µl of water and dialyzed (dialysis buffer: 10 mM Tris-HCl pH7.5, 75 mM NaCl, 0.01 % Triton X-100) for ~6 hr at 4 °C in a MWCO 7,000 Da mini dialysis column (Pierce). The dialyzed sample (90-100 µl) was again completely dried by vacuum evaporation and re-suspended in 20 µl of 0.1 % SDS and 10 mM DTT (prepared from a fresh stock solution). The sample was heated at 95 °C for 5 min and cooled to room temperature. The reduced thiol groups were alkylated by incubating with 0.8 µl of freshly prepared 1M iodoacetamide at room temperature for 45 min in dark. The resulting samples were mixed with 5 µl of 4 x Lammelli SDS load buffer (Bio-Rad) and loaded on 4 %–15 % Mini-PROTEAN TGX gel (Bio-Rad). The samples were migrated until the dye-front had run approximately 1 cm into the gel from the bottom of well. The gel was washed three times with ~200 ml HPLC grade water for 5 min each. The gel piece containing protein was excised and processed for in gel digestion of proteins.

In-Gel Digestion

The gel slices were cut into 1×5×1mm³ dimension and transferred into a 1.5 mL microcentrifuge tube. Samples were washed with water and dehydrated in acetonitrile :50 mM NH₄HCO₃ (1:1 v/v) for 5 minutes and 100% acetonitrile for 30 seconds. Following drying with a vacuum concentrator (Savant), gel slices were rehydrated in 25 mM dithiothreitol in 50 mM NH₄HCO₃ and incubated for 20 min at 56 °C. With the removal of the supernatant, 55 mM iodoacetamide in 50 mM NH₄HCO₃ was added and the samples were incubated in the dark for 20 min at room temperature. Gel slices were washed and dehydrated as described before. Following removal of the liquid by vacuum concentrator, the sample was rehydrated in 12 ng/µL Trypsin Gold (Promega) in 0.01 % ProteaseMAXTM Surfactant (Promega): 50 mM NH₄HCO₃ and incubated at 50 °C for one hr. Condensate was collected by centrifuging at 14,000 × g for 10 seconds and the solution was transferred to a new tube. Trifluoroacetic acid was added to a final

concentration of 0.5 % to inactivate trypsin and the solution was dried by vacuum concentrator.

LC/MS/MS

The LC-MS/MS tryptic digested peptides were dissolved in 0.1 % formic acid (v/v) and loaded at 15 μ L/min for 10 min using a nanoACQUITY C18 Trap column (20 \times 0.18 mm i.d., 5 μ m 100Å C18, Waters, 186007238). Peptides were separated using an EASY-Spray LC Column(150 \times 0.075 mm i.d., 3 μ m 100Å C18, ThermoFisher, ES800) with a gradient using solvent A (0.1 % formic acid in water) and solvent B (0.1 % formic acid in acetonitrile) at a 0.5 μ L/min flow rate. The gradient started with 1 % B for 5 min, followed by 85 min with a linear increase to 35 % B. The gradient was increased to 85 % B in 5 min followed by decreasing back to 1 % B in 5 min as the final wash step. A nanoACQUITY UPLC (Waters) was coupled to a Velos Pro Dual-Pressure Linear Ion Trap mass spectrometer (Thermo Scientific) for data acquisition. A data-dependent acquisition routine was used for a mass spectrum from m/z 300 to 2000 and followed by ten tandem mass spectrometry scans.

Data Analysis

Raw data files were processed using Proteome Discoverer (ThermoFisher). The data were searched against the human Swiss-Port index (09/01/15) using Sequest HT with precursor mass tolerances of 1.5 Da and fragment mass tolerances of 0.8 Da. Maximum missed cleavage sites of full tryptic digestion was two and dynamic modifications of acetylation (N-terminus), carbamidomethylation(cysteine), propionamidation(cysteine) and oxidation(methionine) were considered. The processed mass spectrometry data was analyzed using the Scaffold software (4.4.5). Quantifications from replicate 1 are presented in main figures and from replicate 2 in supplementary figures. For the analysis presented in Figure 1 and S1, spectral quantification was done using the normalized weighted spectral counts with minimum peptide identification threshold at 95 % and protein identification threshold of 95 % with 1 minimum peptide. For analysis presented in Figure 2 and S2, spectral quantification was done using the Normalized Spectral Abundance Factor (NSAF) (Zhang et al.,

2010). A total of 341 (replicate 1) or 259 (replicate 2) proteins were identified at 99 % threshold each with a minimum of 2 peptides. When Scaffold grouped together similar proteins into clusters, only those proteins were retained from a cluster that had non-zero NSAF value in at least one of the four samples. There are several proteins that are detected only in one or the other alternate EJC, and thus had zero values in samples where they were undetected. Also, many EJC specific proteins had zero values in FLAG-only control IPs. A pseudocount of 0.00001 was added to all NSAF values to prevent loss of such proteins when divided by zero. Fold-enrichment over FLAG-only control was calculated for each of the three EJC samples as follows:

Fold-enrichment:

$$\log_2[\text{NSAF}(\text{FLAG-EJC}+0.00001)] / [\text{NSAF}(\text{FLAG-only}+0.00001)]$$

The comparison of fold-enrichment values for all 341 proteins in the EJC core or alternate EJCs was carried out in R package ggplot2 (via scatter plots). Proteins that were >10-fold enriched in one of the three EJC IPs were included in the heatmap (using R package gplots). In this analysis, proteins that most likely were contaminants (e.g. cytoskeleton proteins, histones, metabolic enzymes) were not included in the heatmap but are shown in the >10-fold enrichment table.

Glycerol Gradient Fractionation

Five 15-cm plates with ~90 % confluent HEK293 cells expressing FLAG-tagged MAGOH, CASC3, RNPS1 proteins, or FLAG-peptide as a control, were cultured and induced as above. Cell lysis, FLAG-immunoprecipitation, RNase A digestion and FLAG-elution steps were also carried out as described above. FLAG-IP elution was layered onto pre-cooled continuous 10-30 % glycerol gradients prepared in 11 ml Beckman centrifuge tubes. Gradients were run at 32,000 rpm for 16 hours at 4 °C. Gradients were fractionated by-hand into 500 µl fractions. Proteins were precipitated using TCA and resuspended in 15 µl of 1x SDS loading buffer for analysis on 12 % SDS-PAGEs.

siRNA-mediated Knockdowns

HEK293 siRNA knockdowns

HEK293 cells were seeded into 24-well plates. Cells were transfected 4 hours later following the Mirus TransIT-X2 procedure with 55-60 pmols of control, EIF4A3, CASC3, RNPS1, or UPF1 siRNA. Cells were harvested 48 hr later. Knockdown was checked by Western blot and subsequently purified RNA was used for qRT-PCR analysis. For 96 hr knockdowns, HEK293 cells were transfected as above and were incubated for 24 hr. Cells were transfected again at roughly 70-80 % confluence following the Mirus TransIT-X2 procedure using 50-60 pmol of control, EIF4A3, CASC3, RNPS1, or UPF1 siRNA. Cells were harvested ~48 hr (~96 total hours after first transfection) later. Knockdown was checked by Western blot and subsequently purified RNA was used for qRT-PCR analysis.

HeLa Tet-off siRNA knockdowns and reporter RNA expression

HeLa Tet-off cells in 12-well plates (1.2×10^5 cells/well) were reverse transfected with 15 pmol of control, UPF1, CASC3 and RNPS1 siRNA using RNAiMAX following the manufacturer's protocol. After 24 hr, cells were co-transfected with plasmids (100 ng of pcTET2- β wt β or pcTET2- β 39 β , 30 ng of pc β wtGAP3UAC and 70 ng of pezYFP or carrier DNA) and a second dose of 15 pmol of siRNA using JetPrime (PolyPlus). Tetracycline (50 ng/ml) was included at the time of transfection to repress reporter RNA expression, and was removed 20 hr later to induce reporter RNA expression for 6-8 hr. Cells were harvested in clear sample buffer for western blot analysis and TRIzol extraction of RNA, which was analyzed by Northern Blotting.

Overexpression of alternate EJC factors

HEK293 FLAG-EJC overexpression

HEK293 cells expressing FLAG-tagged CASC3, RNPS1 proteins, or FLAG-peptide as a control, were seeded into 6-well plates. Cells were induced with 625 ng/ml of Doxycycline for 48 hr. Overexpression was checked by Western blot and subsequently purified RNA was used for qRT-PCR analysis.

For IPs following alternate EJC protein overexpression, HEK293 cells stably expressing FLAG-tagged CASC3 or RNPS1, or FLAG-peptide as a control, were seeded in 10 cm plates and induced with 625 ng/ml of Doxycycline for 48 hr. Endogenous RBM8A or EIF4A3 IPs were carried out as described above.

HEK293 EIF4A3 or EIF4A3 YRAA Rescue

HEK293 cells were seeded into 24-well plates. Cells were transfected 4 hr later following the Mirus TransIT-X2 procedure with 60 pmol of control, or EIF4A3 siRNA, and 300 ng of pcDNA3 empty, FLAG-EIF4A3 wt or FLAG-EIF4A3 YRAA and 200 ng of pcDNA3 vector. Cells were harvested ~48 hr later. Knockdown and EIF4A3 expression was checked by Western blot and subsequently purified RNA was used for qRT-PCR analysis.

HEK293 cells were seeded into 6-well plates. Cells were transfected four hours later following the Mirus TransIT-X2 protocol with 300 ng of pcDNA3 empty, FLAG-EIF4A3 wt or FLAG-EIF4A3 YRAA and 200 ng of pcDNA3 vector. Cells were harvested in 1x PBS 48 hr later and washed for subsequent FLAG IP as previously described.

β -globin NMD assays

The pulse-chase experiments were performed in HeLa Tet-off cells as described previously (Singh et al., 2007). Briefly, cells growing in 12-well plates were transfected with 10 ng of pc β wtGAP3UAC, 200 ng of pcTET2- β 39 β and 250 ng of pezFLAG-CASC3 (or pezFLAG empty vector) in the presence of 50 ng/ml tetracycline. 36 hr later, expression of β 39 mRNA was induced for 6 hr by removing Tet, and then suppressed again via addition of 1 μ g/ml Tet. Time points were collected starting ~30 min after addition of Tet for 0 hr time point. Total RNA was extracted using TRIzol and one-half of the RNA sample was analyzed by Northern blots. The autoradiogram signal was scanned using Fuji FLA imager, and quantified using ImageQuant software.

For steady-state assays, HeLa CCL2 cells growing in 12-well plates were transfected with 100 ng of pc β wtGAP3UAC, 100 ng of either pc β wt β or pc β 39 β , and 150 ng of pezFLAG plasmids (expressing RNPS1 or CASC3, or empty vector as a

control). Cells were harvested 48 hr post-transfections and total RNA extracted was analyzed by Northern blots.

qRT-PCR

RNA was isolated from cells using Trizol, DNase treated, purified with Phenol:Chloroform:Isoamyl alcohol (25:24:1, pH 4.5) and resuspended in RNase-free water. RNA was reverse transcribed using oligo-dT (Promega) and Superscript III (Invitrogen). After reverse transcription of RNA the samples were treated with RNase H (Promega) for 30 min at 37 °C. The samples were then diluted to 5 ng/μl before proceeding to qPCR setup. For each qPCR 25 ng of cDNA was mixed with 7.5 μl of 2 x SYBR Green Master Mix (ABS), 0.6 μl of a 10 mM forward and reverse primer mix (defrosted once), and quantity sufficient water for a 15 μl reaction volume. The qPCRs were performed on (Applied Biosystems) in triplicates (technical). Parallel with NMD targets, β-actin or TATA-binding protein (TBP) were used as internal controls. Fold-change calculations were performed by delta-delta Ct method. Fold-change from at least three biological replicates were used to determine the standard error of means. The p-values were calculated using student's t-test.

Cytoplasmic FLAG-IPs of alternate EJCs

One 15-cm plate of HEK293 cells expressing FLAG-tagged MAGOH, CASC3, RNPS1 proteins, or FLAG-peptide as a control, were cultured and induced as above. Cells were lysed in 2 ml RSB-150 buffer [10 mM Tris-HCl pH 7.5, 150 mM NaCl, 5 mM MgCl₂, 10 μg/ml Aprotinin, 10 μM Leupeptin, 1 μM Pepstatin, 1 mM PMSF] supplemented with 0.05 % digitonin and 1 mM DTT. Lysates were passed through a 25 gauge needle 5 times before centrifugation at 3,000 x g for 1 min at 4 °C. Supernatant was removed and centrifuged at 21,000 x g for 10 min at 4 °C, and passed through a 0.45 μm filter (Cytoplasmic Fraction). The first pellet was resuspended in RSB-150 and pelleted again at 3,000 x g for 1 min at 4 °C to remove residual cytoplasmic contaminants. The nuclei were then resuspended in 2 ml RSBT (components) and sonicated as previously described, before being centrifuged and purified as done for the cytoplasmic fraction.

Approximately 2 ml of each fraction were collected and used for FLAG-IP as described above.

RIPiT-Seq data analysis

Alternate EJC RIPiTs from HEK293 cells

RIPiTs were carried out with and without formaldehyde crosslinking as described previously (Singh et al., 2014) with the following modifications. For native RIPiTs, total extracts from four 15-cm plates prepared in hypotonic lysis buffer supplemented with 150mM NaCl-containing were used as input into FLAG-IP. For formaldehyde crosslinked RIPiTs, total extracts were prepared from six 15-cm plates in denaturing lysis buffer supplemented with 150 mM NaCl-containing for input into FLAG-IP. Following IP and washes, RNase I (0.006 U/ml in Isotonic wash buffer (IsoWB)) treatments were performed at 4 °C for 10 min. For the second IP, the following antibodies conjugated to protein-A Dynabeads were used: anti-EIF4A3 (Bethyl A302-980A, 10 µg/RIPiT), anti-CASC3 (Bethyl A302-472A, 2 µg/RIPiT), anti-RNPS1 (HPA044014-100UL, 2 µg/RIPiT). RIPiTs were eluted in clear sample buffer and divided into two parts for RNA and protein analysis as described previously. RIPiTs to enrich EJC footprints upon cycloheximide (CHX) treatment were carried out as above except that cells were incubated with 100 µg/ml CHX for 3 hr prior to harvesting. CHX was included at the same concentration in PBS (for washes before lysis) and cell lysis buffers.

High-throughput sequencing library preparation

For RIPiT-Seq, RNA extracted from ~80 % of RIPiT elution was used to generate strand-specific libraries using a custom library preparation method as detailed in (Gangras et al., 2018). For RNA-Seq libraries, 5 µg of total cellular RNA was used as input for ribosomal RNA depletion (Ribozero, Illumina). Purified RNA was then used to generate strand-specific libraries using a custom library preparation method (Gangras et al., 2018). Following PCR amplification, all libraries were quantified using Bioanalyzer

(DNA lengths) and Qubit (DNA amounts). Libraries were sequenced on Illumina HiSeq 2500 in the single-end format (50 and 100 nt read lengths).

Data pre-processing

Adapter trimming and PCR duplicate removal

After demultiplexing, fastq files containing unmapped reads were first trimmed using cutadapt. A 12 nt sequence on read 5' ends consisting of a 5 nt random sequence, 5 nt identifying barcode, and a CC was removed with the random sequence saved for each read for identifying PCR duplicates down the line. Next as much of the 3'-adapter (miR-Cat22) sequence TGAATTCTCGGGTGCCAAGG was removed from the 3' end as possible. Any reads less than 20 nt in length after trimming were discarded.

Alignment and removal of multimapping reads

Following trimming reads were aligned with tophat v2.1.1 (Trapnell et al., 2009) using 12 threads to NCBI GRCh38 with corresponding Bowtie2 index. After alignment reads with a mapping score less than 50 (uniquely mapped) were removed, i.e. all multimapped reads were discarded. Finally all reads mapping to identical regions were compared for their random barcode sequence; if the random sequences matched, such reads were inferred as PCR duplicates and only one such read was kept.

Removal of stable RNA mapping reads

Next, reads which came from stable RNA types were counted and removed as follows. All reads were checked for overlap against hg38 annotations for miRNA, rRNA, tRNA, scaRNA, snoRNA, and snRNA using bedtools intersect (Quinlan and Hall, 2010), and any reads overlapping by more than 50 % were removed. Reads aligned to chrM (mitochondrial) were also counted and removed.

Human reference transcriptome

The primary reference transcriptome used in all post-alignment analysis was obtained from the UCSC Table Browser. CDS, exon, and intron boundaries were obtained for

canonical genes by selecting Track: Gencode v24, Table: knownGene, Filter: knownCanonical (describes the canonical splice variant of a gene).

Read distribution assignment

Fractions of reads corresponding to exonic, intronic, intergenic, and canonical EJC and non-canonical EJC regions were then computed. Exonic regions were defined by the canonical hg38 genes, with intronic regions defined as the regions between exons in said genes. Bedtools intersect was used to compare reads against these exon and intron annotations, and reads which overlapped the annotation by more than 50 % were counted. Any reads which did not overlap either the exon or intron annotations sufficiently were counted as intergenic. For classification of reads as canonical versus non-canonical EJC footprints, the canonical region for each library was defined using the meta-exon distribution at exon 3'-ends (Figure 3C and S3J). All reads with their 5' ends falling within the window starting at -24 position till the 25 % max height on the 5' side of the canonical EJC peak were counted as canonical reads. Similarly any read whose 5' end was found anywhere between the start of the exon and 10 bp upstream of that 25 % max point was considered non-canonical.

k-mer analysis

Lists of all 6-mers and 3-mers present in reads mapping to exonic regions (as described above) were produced for each RIPiT-Seq sample. The ratio of total 3-mer frequency in RIPiT-Seq samples to RNA-Seq samples was then used to identify 3-mers enriched in alternate EJCs.

Motif enrichment analysis

Motif enrichment analysis was performed by first selecting RNA binding proteins of interest - namely SR proteins - from the position weight matrices (PWMs) available on <http://rbpdb.ccb.utoronto.ca/>. For all reads mapped to exonic regions, a score was then generated representing the highest possible binding probability for each protein on that read. For visualization the cumulative distribution of these score frequencies was plotted for both pull down and RNA-Seq replicates, with a relatively higher score frequency at a

positive score implying greater binding affinity. The p-values between RIPiT-Seq and RNA-Seq replicates were also computed for every score using a negative binomial based model, with significant values primarily in positive score regions implying a binding preference for that protein.

Differential enrichment analysis

Differential analysis of exons and transcripts between CASC3 and RNPS1 pull down was conducted with the DESeq2 (Love et al., 2014) package in R. Exons and transcripts with significant differential expression ($p < 0.05$) were selected. All the following analysis was conducted using only the lists of significantly differentially expressed transcripts, unless otherwise noted.

Estimation of nuclear versus cytoplasmic levels

Nuclear and cytoplasmic RNA levels were estimated by first obtaining nuclear and cytoplasmic reads from (Neve et al., 2016). Reads were aligned and mapped to our exonic annotation as described above, and a ratio of nuclear to cytoplasmic reads was then calculated for all transcripts.

Comparison to genes with detained introns

A list of detained and non-detained introns was obtained from (Boutz et al., 2015). To identify detained intron containing and lacking genes in our RNA-Seq data, we carried out analysis using a DESeq2-based pipeline as described by Boutz *et al.* Briefly, using two RNA-Seq replicates we first created artificial data sets containing the same numbers of total reads per replicate, but with counts originating from introns in a given gene spread evenly amongst those introns in the artificial set. By comparing the intron distributions of these artificial replicates to the experimental replicates using DESeq we were able to produce lists of detained introns (introns with significantly ($p < 0.05$) higher expression levels compared to the artificially spread data) and non-detained introns (introns with non-significant ($p > 0.1$) expression levels compared to the artificially spread data). The transcripts containing introns found to be detained/non-detained in both our analysis and the analysis done by Boutz *et al.* make up the stringent lists,

which were used for analysis in Figure 4D. Of the 693 canonical genes containing detained introns reported by Boutz et al. we found 555 in our own analysis (80 %) and of the 5294 canonical genes lacking detained introns we found 812 (15 %).

Features compared between two alternate EJC sets

mRNA half life data was taken from (Tani et al., 2012) with no further processing on our part. Translation efficiency data was similarly obtained from (Kiss et al., 2017).

Gene ontology analysis

DAVID gene ontology tool (Huang et al., 2009) was used to compare the set of genes (canonical Ensembl transcript IDs) predicted by DESeq2 analysis to be significantly enriched in CASC3 or RNPS1 EJCs against a background list containing only those human genes that were reliably detected by DESeq2 (all genes for which DESeq2 calculated adjusted p-values). Only non-redundant categories with lowest p-value (with Benjamini-Hochberg correction) are reported.